NASA/TM—2012-217676

Simulations of Spray Reacting Flows in a Single Element LDI Injector With and Without Invoking an Eulerian Scalar PDF Method

Tsan-Hsing Shih
Ohio Aerospace Institute, Brook Park, Ohio

Nan-Suey Liu
Glenn Research Center, Cleveland, Ohio

August 2012

NASA STI Program . . . in Profile

Since its founding, NASA has been dedicated to the advancement of aeronautics and space science. The NASA Scientific and Technical Information (STI) program plays a key part in helping NASA maintain this important role.

The NASA STI Program operates under the auspices of the Agency Chief Information Officer. It collects, organizes, provides for archiving, and disseminates NASA's STI. The NASA STI program provides access to the NASA Aeronautics and Space Database and its public interface, the NASA Technical Reports Server, thus providing one of the largest collections of aeronautical and space science STI in the world. Results are published in both non-NASA channels and by NASA in the NASA STI Report Series, which includes the following report types:

- TECHNICAL PUBLICATION. Reports of completed research or a major significant phase of research that present the results of NASA programs and include extensive data or theoretical analysis. Includes compilations of significant scientific and technical data and information deemed to be of continuing reference value. NASA counterpart of peer-reviewed formal professional papers but has less stringent limitations on manuscript length and extent of graphic presentations.

- TECHNICAL MEMORANDUM. Scientific and technical findings that are preliminary or of specialized interest, e.g., quick release reports, working papers, and bibliographies that contain minimal annotation. Does not contain extensive analysis.

- CONTRACTOR REPORT. Scientific and technical findings by NASA-sponsored contractors and grantees.

- CONFERENCE PUBLICATION. Collected papers from scientific and technical conferences, symposia, seminars, or other meetings sponsored or cosponsored by NASA.

- SPECIAL PUBLICATION. Scientific, technical, or historical information from NASA programs, projects, and missions, often concerned with subjects having substantial public interest.

- TECHNICAL TRANSLATION. English-language translations of foreign scientific and technical material pertinent to NASA's mission.

Specialized services also include creating custom thesauri, building customized databases, organizing and publishing research results.

For more information about the NASA STI program, see the following:

- Access the NASA STI program home page at *http://www.sti.nasa.gov*

- E-mail your question to *help@sti.nasa.gov*

- Fax your question to the NASA STI Information Desk at 443–757–5803

- Phone the NASA STI Information Desk at 443–757–5802

- Write to:
  STI Information Desk
  NASA Center for AeroSpace Information
  7115 Standard Drive
  Hanover, MD 21076–1320

NASA/TM—2012-217676

Simulations of Spray Reacting Flows in a Single Element LDI Injector With and Without Invoking an Eulerian Scalar PDF Method

Tsan-Hsing Shih
Ohio Aerospace Institute, Brook Park, Ohio

Nan-Suey Liu
Glenn Research Center, Cleveland, Ohio

National Aeronautics and
Space Administration

Glenn Research Center
Cleveland, Ohio 44135

August 2012

Acknowledgments

This work is supported by the NASA Fundamental Aeronautics Program. The authors would like to thank Drs. Thomas Wey, Jeff Moder and M.S. Raju for their technical help on the Eulerian scalar PDF solver. The authors would also like to express our thanks to Professor John L. Lumley, Professor Zellman Warhaft and Professor J. Y. Chen for their critical comments, suggestions and encouragements to our previous related work on "Conservation PDF Equations of Turbulence" that lead to our current work. Finally, we would like to thank Professor Stephen B. Pope for his excellent text book "Turbulent Flows" that guides us in our PDF studies and this work.

This work was sponsored by the Fundamental Aeronautics Program at the NASA Glenn Research Center.

Level of Review: This material has been technically reviewed by technical management.

Available from

NASA Center for Aerospace Information
7115 Standard Drive
Hanover, MD 21076–1320

National Technical Information Service
5301 Shawnee Road
Alexandria, VA 22312

Available electronically at http://www.sti.nasa.gov

Contents

Simulations of Spray Reacting Flows in a Single Element LDI Injector With and Without Invoking an Eulerian Scalar PDF Method

Tsan-Hsing Shih
Ohio Aerospace Institute
Brook Park, Ohio 44142

Nan-Suey Liu
National Aeronautics and Space Administration
Glenn Research Center
Cleveland, Ohio 44135

Abstract

This paper presents the numerical simulations of the Jet-A spray reacting flow in a single element lean direct injection (LDI) injector by using the National Combustion Code (NCC) with and without invoking the Eulerian scalar probability density function (PDF) method. The flow field is calculated by using the Reynolds averaged Navier-Stokes equations (RANS and URANS) with nonlinear turbulence models, and when the scalar PDF method is invoked, the energy and compositions or species mass fractions are calculated by solving the equation of an ensemble averaged density-weighted fine-grained probability density function that is referred to here as the averaged probability density function (APDF). A nonlinear model for closing the convection term of the scalar APDF equation is used in the presented simulations and will be briefly described. Detailed comparisons between the results and available experimental data are carried out. Some positive findings of invoking the Eulerian scalar PDF method in both improving the simulation quality and reducing the computing cost are observed.

1.0 Introduction

Many engineering applications of the computational fluid dynamics (CFD) for internal combustor flows need to accurately account for the turbulence-chemistry interaction to facilitate a higher fidelity analysis of the design. In the conventional CFD simulation methods that involve an averaging procedure (e.g., RANS and URANS) or filtering process (e.g., large eddy simulation LES), the turbulence-chemistry interaction manifests itself as an unclosed term that must be modeled. Various such models have been proposed. The simplest one is the so called "laminar chemistry" which simply ignores the effects of the fluctuations of turbulence on the chemical reactions. However, in the PDF simulation methods (no matter Lagrangian or Eulerian approach, joint or scalar PDF), the chemical reaction source term in the PDF equations is always in a closed form, therefore it can be directly calculated without any modeling (Ref. 1). This unique feature will stay when the PDF method is extended to its large eddy simulation (LES) approach (Ref. 2).

In this paper, we present the preliminary numerical results of the complex spray reacting flow in a single element LDI injector. The simulation methods include both the conventional CFD methods (RANS, URANS) and an Eulerian scalar PDF method (Ref. 3), in which the velocity field is determined by the continuity and momentum equations of averaged Navier-Stokes equations. All simulations are done with the NCC code (Ref. 4) using the same numerical parameter setting and the same computational domain and grid resolution. In the RANS and URANS simulations, all the turbulent flux models, i.e., Reynolds stresses, heat and species fluxes, are nonlinear models (Ref. 5 and 6). The basic equations and models are described in Section 2.0. In the Eulerian scalar PDF method, we solve the transport equation of scalar APDF. It should be mentioned that the joint APDF equation for velocity and species is generally

in a closed form (Ref. 7). However, for the marginal or scalar APDF equation, the convection term contains a conditional mean that needs to be modeled. Here a nonlinear model is introduced, which provides a diffusion process in the sample variable space. The brief description about the scalar APDF equation and model is given in Section 3.0.

The liquid fuel is Jet-A, and C12H23 is adopted as its surrogate. At this stage of the simulations, we use a relatively simple spray injection model (i.e., prescribed droplet size and distribution) and a global five-species one-step kinetics for combustion chemistry (Ref. 8), so that we could concentrate more on the evaluation of different simulation approaches.

The main results of steady simulations, including both with and without invoking an Eulerian scalar PDF method, are described in Section 4.1. They are compared side by side to examine how much effects are produced by the invoked scalar PDF method. The results for unsteady simulations are described in a similar manner in Section 4.2.

One of the main objectives of this study is to search for a consistent and stable simulation tool for multiphase combustion flows. We require that this tool is not only to have the "physics" based models but is also able to produce the physically reasonable, numerically stable solution that can be sustained over a very long (infinite) time period. And also, this tool should be relatively economic. It is encouraging to observe from the present simulations that the adopted Eulerian scalar PDF method does show the potential for improving the simulation quality and also reducing the computing cost.

2.0 Basic Equations for RANS and URANS Simulations

2.1 Averaged Turbulent Variables $\overline{\phi}(\boldsymbol{x},t)$, $\tilde{\phi}(\boldsymbol{x},t)$

In the case of compressible turbulent reacting flow, we often deal with two types of ensemble averaging: one with the density weighting, the other without the density weighting. The averaged turbulent variable without the density weighting is denoted by $\overline{\phi}(\boldsymbol{x},t)$ and is defined as

$$\overline{\phi}(\boldsymbol{x},t) = \lim_{N\to\infty} \frac{1}{N}\sum_{n=1}^{N} \phi^{(n)}(\boldsymbol{x},t) \tag{1}$$

where $\phi^{(n)}$ is the *n-th* independent realization of turbulent variables, i.e., velocity components $U_i^{(n)}$, density $\rho^{(n)}$, pressure $P^{(n)}$, *m-th* species mass fractions $\Phi_m^{(n)}$ and internal energy $e^{(n)} = \sum_{m=1}^{M} \Phi_m^{(n)} e_m^{(n)}$. N is the total number of independent realizations. The density-weighted averaged turbulent variable is denoted by $\tilde{\phi}(\boldsymbol{x},t)$ and is defined as

$$\tilde{\phi}(\boldsymbol{x},t) = \frac{\overline{\rho\phi}}{\overline{\rho}} \tag{2}$$

These ensemble averaged variables $\overline{\phi}(\boldsymbol{x},t)$, $\tilde{\phi}(\boldsymbol{x},t)$ represent the turbulent mean variables that can be actually measured in experiments. They are deterministic in nature. They can vary with the time and space but usually contain relatively low frequencies and low wave numbers of the turbulent mean flow, when compared with the ones contained in the non-averaged turbulent variables $\phi(\boldsymbol{x},t)$.

2.2 Basic Equation

Applying the ensemble averaging, Equations (1) and (2), to the compressible Navier-Stokes equations, we will obtain:

$$\frac{\partial \overline{\rho}}{\partial t} + \frac{\partial \overline{\rho}\widetilde{U}_j}{\partial x_j} = 0 \tag{3}$$

$$\frac{\partial \overline{\rho}\widetilde{U}_i}{\partial t} + \frac{\partial \overline{\rho}\widetilde{U_i U_j}}{\partial x_j} = -\frac{\partial \overline{P}}{\partial x_i} + \frac{\partial}{\partial x_j}\left(\overline{2\rho\nu(S_{ij} - \frac{1}{3}\delta_{ij}S_{kk})}\right) \tag{4}$$

$$\frac{\partial \overline{\rho}\tilde{e}}{\partial t} + \frac{\partial \overline{\rho}\widetilde{U_i e}}{\partial x_i} = -\frac{\partial \overline{q}_i}{\partial x_i} + \overline{PS_{kk}} + \overline{2\rho\nu\left(S_{ij}S_{ij} - \frac{1}{3}S_{ii}S_{kk}\right)} + \overline{Q} \tag{5}$$

$$\frac{\partial \overline{\rho}\widetilde{\Phi}_m}{\partial t} + \frac{\partial \overline{\rho}\widetilde{U_i\Phi_m}}{\partial x_i} = \frac{\partial}{\partial x_i}\left(\overline{\rho\Gamma^{(m)}\frac{\partial \Phi_m}{\partial x_i}}\right) + \overline{W}_m \qquad m = 1,2,\cdots,M \tag{6}$$

where

$$\overline{P} = \overline{\rho}R\sum_{m=1}^{M}\frac{\widetilde{\Phi_m T}}{w_m} = \frac{\overline{\rho}R}{c_v}\sum_{m=1}^{M}\frac{\widetilde{\Phi_m e}}{w_m}, \text{ or } \overline{P} = \frac{\overline{\rho}R}{c_v}\sum_{m=1}^{M}\frac{\widetilde{\Phi_m\Phi_{M+1}}}{w_m} \tag{7}$$

$$\overline{q}_i = -\overline{\rho\kappa c_\upsilon\frac{\partial T}{\partial x_i}} - \sum_{m=1}^{N}\overline{\rho\Gamma^{(m)}h_m\frac{\partial \Phi_m}{\partial x_i}} \tag{8}$$

In the above equations, κ, ν and $\Gamma^{(m)}$ are the molecular heat conductivity, kinematic viscosity and the *m-th* species diffusivity, they have the same dimension (i.e., velocity · length). It is commonly assumed that $\Gamma^{(m)}$ is the same for all species Φ_m, and w_m is the molecular weight. The h_m, T are the enthalpy of species and the temperature, Q is the radiation rate, $W_m = \rho S_m$ is the chemical production rate of the *m-th* species, Φ_{M+1} represents the internal energy e, R is the universal gas constant. These equations are general; however, unlike the constant density flows, further approximations for the terms on their right hand side are required in order to complete the density weighted ensemble averaging process. One of such approximations leads to

$$\overline{2\rho\nu\left(S_{ij} - \frac{1}{3}\delta_{ij}S_{kk}\right)} \approx \mu\left(\frac{\partial \widetilde{U}_i}{\partial x_j} + \frac{\partial \widetilde{U}_j}{\partial x_i} - \frac{2}{3}\delta_{ij}\frac{\partial \widetilde{U}_k}{\partial x_k}\right) \tag{9}$$

In which, we have basically neglected the variations of μ and ρ during the averaging process, the value of μ will be considered as a function of $\overline{P}, \widetilde{T}, \cdots$. Other types of approximations are also possible, for example,

$$\overline{2\rho\nu\left(S_{ij} - \frac{1}{3}\delta_{ij}S_{kk}\right)} \approx \nu\left(\frac{\partial \overline{\rho}\widetilde{U}_i}{\partial x_j} + \frac{\partial \overline{\rho}\widetilde{U}_j}{\partial x_i} - \frac{2}{3}\delta_{ij}\frac{\partial \overline{\rho}\widetilde{U}_k}{\partial x_k}\right) \tag{10}$$

Similarly,

$$\overline{q}_i = -\overline{\rho\kappa c_\upsilon \frac{\partial T}{\partial x_i}} - \sum_{m=1}^{M} \overline{\rho\Gamma^{(m)} h_m \frac{\partial \Phi_m}{\partial x_i}} \approx -\kappa c_\upsilon \frac{\partial \overline{\rho}\widetilde{T}}{\partial x_i} - \sum_{m=1}^{M} \Gamma^{(m)} \overline{\rho}\, \widetilde{h_m \frac{\partial \Phi_m}{\partial x_i}} \tag{11}$$

$$\overline{\rho\Gamma^{(m)} \frac{\partial \Phi_m}{\partial x_i}} \approx \Gamma^{(m)} \frac{\partial \overline{\rho}\widetilde{\Phi}_m}{\partial x_i} \tag{12}$$

Where ν, κ, c_υ, and $\Gamma^{(m)}$ are considered as functions of $\overline{P}, \widetilde{T}, \cdots$. Furthermore, we invoke the dissipation rate of turbulent kinetic energy,

$$\overline{2\rho\nu\left(S_{ij}S_{ij} - \frac{1}{3}S_{ii}S_{kk}\right)} \equiv \overline{\rho}\,\tilde{\varepsilon} \tag{13}$$

Therefore, the ensemble averaged compressible Navier-Stokes equations can be written as

$$\frac{\partial \overline{\rho}}{\partial t} + \frac{\partial \overline{\rho}\widetilde{U}_j}{\partial x_j} = 0 \tag{14}$$

$$\frac{\partial \overline{\rho}\widetilde{U}_i}{\partial t} + \frac{\partial \overline{\rho}\widetilde{U_i U_j}}{\partial x_j} = -\frac{\partial \overline{P}}{\partial x_i} + \frac{\partial}{\partial x_j}\left[\nu\left(\frac{\partial \overline{\rho}\widetilde{U}_i}{\partial x_j} + \frac{\partial \overline{\rho}\widetilde{U}_j}{\partial x_i} - \frac{2}{3}\delta_{ij}\frac{\partial \overline{\rho}\widetilde{U}_k}{\partial x_k}\right)\right] \tag{15}$$

$$\frac{\partial \overline{\rho}\tilde{e}}{\partial t} + \frac{\partial \overline{\rho}\widetilde{U_i e}}{\partial x_i} = -\frac{\partial \overline{q}_i}{\partial x_i} + \overline{PS_{kk}} + \overline{\rho}\,\tilde{\varepsilon} + \overline{Q} \tag{16}$$

$$\frac{\partial \overline{\rho}\widetilde{\Phi}_m}{\partial t} + \frac{\partial \overline{\rho}\widetilde{U_i \Phi_m}}{\partial x_i} = \frac{\partial}{\partial x_i}\left(\Gamma^{(m)} \frac{\partial \overline{\rho}\widetilde{\Phi}_m}{\partial x_i}\right) + \overline{\rho}\widetilde{S}_m \qquad m = 1, 2, \cdots, M \tag{17}$$

$$\overline{P} = \overline{\rho}R\sum_{m=1}^{M}\frac{\widetilde{\Phi_m T}}{w_m} = \frac{\overline{\rho}R}{c_v}\sum_{m=1}^{M}\frac{\widetilde{\Phi_m e}}{w_m}, \text{ or } \overline{P} = \frac{\overline{\rho}R}{c_v}\sum_{m=1}^{M}\frac{\widetilde{\Phi_m \Phi_{M+1}}}{w_m} \tag{18}$$

$$\overline{q}_i = -\kappa c_\upsilon \frac{\partial \overline{\rho}\widetilde{T}}{\partial x_i} - \sum_{m=1}^{M} \overline{\rho}\,\Gamma^{(m)} \widetilde{h_m \frac{\partial \Phi_m}{\partial x_i}} \tag{19}$$

These equations are considered quite general, because i) they are exact if the flow becomes incompressible, ii) all the approximations made in Equations (15), (16) and (17) are related only to the molecular diffusion terms which are less important and even become negligibly small, i.e., they are of O(1/Re) comparing with the convection terms on the left hand side for turbulent flows at high Reynolds numbers (see Ref. 9 and 1). For the steady and unsteady simulations (i.e., RANS and URANS), Equation (14) to (17) are often used together with the further approximations for Equations (18) and (19):

$$\overline{P} = \overline{\rho R\sum_{m=1}^{M}\frac{\Phi_m T}{w_m}} = \overline{\left(\frac{\rho RT}{\overline{M}}\right)} \approx \frac{\overline{\rho}R\widetilde{T}}{\widetilde{M}}, \quad \frac{1}{\overline{M}} = \sum_{m=1}^{M}\frac{\Phi_m}{w_m}, \quad \frac{1}{\widetilde{M}} = \sum_{m=1}^{M}\frac{\widetilde{\Phi}_m}{w_m} \tag{20}$$

$$\overline{q}_i = -\kappa c_\upsilon \frac{\partial \overline{\rho}\tilde{T}}{\partial x_i} \tag{21}$$

The momentum flux $\overline{\rho}\widetilde{U_i U_j}$, the energy flux.. and the species flux $\overline{\rho}\widetilde{U_i \Phi}_m$ are considered to be critically important and should be carefully modeled. Many models in the literature, from the simplest zero-equation model (Ref. 10) to the complex two-equation nonlinear models (Refs. 11and 12), have been suggested in terms of turbulent stresses and turbulent scalar fluxes: $\tau_{ij} \equiv \overline{\rho}(\widetilde{U_i U_j} - \tilde{U}_i \tilde{U}_j)$, $\Theta_i \equiv \overline{\rho}(\widetilde{U_i \theta} - \tilde{U}_i \tilde{\theta})$, where θ represents the scalar quantities: e and Φ_m.

2.3 Nonlinear Closure Models for Turbulent Fluxes

A general constitutive relationship between turbulent stresses τ_{ij} and the strain rate of mean turbulence $\tilde{S}_{ij}$, $\tilde{\Omega}_{ij}$ suggests (Ref. 13)

$$\begin{aligned}
\tau_{ij} = & -2C_\mu \overline{\rho}\frac{k^2}{\varepsilon}\left(\tilde{S}_{ij} - \delta_{ij}\tilde{S}_{kk}/3\right) + \frac{1}{3}\delta_{ij}\tau_{kk} \\
& - A_3 \overline{\rho}\frac{k^3}{\varepsilon^2}\left(\tilde{S}_{ik}\tilde{\Omega}_{kj} - \tilde{\Omega}_{ik}\tilde{S}_{kj}\right) \\
& + 2A_5 \overline{\rho}\frac{k^4}{\varepsilon^3}\left[\tilde{\Omega}_{ik}\tilde{S}_{kj}^2 - \tilde{S}_{ik}^2\tilde{\Omega}_{kj} + \tilde{\Omega}_{ik}\tilde{S}_{km}\tilde{\Omega}_{mj} - \tilde{\Omega}_{kl}\tilde{S}_{lm}\tilde{\Omega}_{mk}\delta_{ij}/3 + II_s(\tilde{S}_{ij} - \delta_{ij}\tilde{S}_{kk}/3)\right],
\end{aligned} \tag{22}$$

where, $\tilde{S}_{ij} = \left(\widetilde{U}_{i,j} + \widetilde{U}_{j,i}\right)/2$, $\tilde{\Omega}_{ij} = \left(\widetilde{U}_{i,j} - \widetilde{U}_{j,i}\right)/2$, $II_s = \left(\tilde{S}_{kk}\tilde{S}_{mm} - \tilde{S}_{kl}\tilde{S}_{lk}\right)/2$. The model coefficients C_μ, A_3 and A_5 are constrained by the realizability condition and the rapid distortion theory limit. They are formulated as (see Ref. 12):

$$C_\mu = \frac{1}{4.0 + A_s\frac{k}{\varepsilon}U^*}, \quad A_3 = \frac{\sqrt{1.0 - A_s^2 C_\mu^2\left(\frac{k}{\varepsilon}S^*\right)^2}}{0.5 + 1.5\frac{k^2}{\varepsilon^2}\Omega^* S^*}, \quad A_5 = \frac{1.6C_\mu\overline{\rho}\frac{k^2}{\varepsilon}}{\overline{\rho}\frac{k^4}{\varepsilon^3}\frac{7S^*S^* + \Omega^*\Omega^*}{4}}, \tag{23}$$

in which,

$$A_s = \sqrt{6}\cos\varphi, \quad \varphi = \frac{1}{3}\arccos\left(\sqrt{6}W^*\right), \quad W^* = \frac{S_{ij}^* S_{jk}^* S_{ki}^*}{(S^*)^3}, \tag{24}$$

$$U^* = \sqrt{(S^*)^2 + (\Omega^*)^2}, \quad S^* = \sqrt{S_{ij}^* S_{ij}^*}, \quad \Omega^* = \sqrt{\tilde{\Omega}_{ij}\tilde{\Omega}_{ij}}, \quad S_{ij}^* = \tilde{S}_{ij} - \frac{1}{3}\delta_{ij}\tilde{S}_{kk} \tag{25}$$

Note, here S_{ij}^* is a zero trace strain rate tensor. Similarly, the nonlinear model for scalar fluxes is formulated as (Ref. 14)

$$\Theta_i = -\vartheta_T\frac{\partial\overline{\rho}\tilde{\theta}}{\partial x_i} - \vartheta_T\frac{k}{\varepsilon}\left(c_1\tilde{S}_{ij} + c_2\tilde{\Omega}_{ij}\right)\frac{\partial\overline{\rho}\tilde{\theta}}{\partial x_j} \tag{26}$$

Where ϑ_T denotes the turbulent diffusivity for the corresponding scalar quantity θ. It is often approximated by $\vartheta_T = \nu_T / \mathrm{Pr}^{\theta}$, and Pr^{θ} represents the turbulent Prandtl number or Schmidt number depending on whether the scalar quantity $\tilde{\theta}$ is the energy $\tilde{e}$ or the species $\tilde{\Phi}_m$. The turbulent eddy viscosity is defined as $\nu_T = C_\mu \cdot k^2 / \varepsilon$. The coefficients, c_1 and c_1, are yet to be calibrated. In the current simulations they are set to be $c_1 = c_2 = -0.24$

The turbulent kinetic energy and its dissipation rate k, ε will be determined from the following model equations:

$$\frac{\partial}{\partial t}\bar{\rho}k + \frac{\partial}{\partial x_i}\bar{\rho}\tilde{u}_i k = \frac{\partial}{\partial x_i}\left[\left(\mu + \mu_T\right)\frac{\partial}{\partial x_i}k\right] - \tau_{ij}\tilde{s}_{ij} - \bar{\rho}\varepsilon \tag{27}$$

$$\frac{\partial}{\partial t}\bar{\rho}\varepsilon + \frac{\partial}{\partial x_i}\bar{\rho}\tilde{u}_i \varepsilon = \frac{\partial}{\partial x_i}\left[\left(\mu + \mu_T\right)\frac{\partial}{\partial x_i}\varepsilon\right] - C_{\varepsilon 1}\tau_{ij}\tilde{s}_{ij}\frac{\varepsilon}{k} - C_{\varepsilon 2}\frac{\bar{\rho}\varepsilon^2}{k} \tag{28}$$

where $C_{\varepsilon 1}$ and $C_{\varepsilon 2}$ are the model coefficients. We have adopted the commonly used values of $C_{\varepsilon 1} = 1.45$ and $C_{\varepsilon 2} = 1.92$ in the present work while keeping in mind that they can be further constructed as functions of the local turbulence quantities (Ref. 15).

3.0 Basic Equation for Scalar Averaged Probability Density Function (APDF)

In this section, we will use the fine grained probability density function (FG-PDF) to define the averaged probability density function (APDF), then explore the relationship between APDF and the ensemble averaged turbulent scalar variables. This will provide the basis for establishing the transport equation for scalar APDF.

3.1 APDF for Scalars

3.1.1 Fine Grained Probability Density Function (FG-PDF) for Scalars $f'_\Phi(\boldsymbol{\psi}; \boldsymbol{x}, t)$

According to Pope's definition (Ref. 1), the joint FG-PDF for turbulent velocity and scalars (i.e., compositions or species mass fractions, internal energy) can be written as

$$f'(\boldsymbol{V}, \boldsymbol{\psi}; \boldsymbol{x}, t) \equiv \delta\left(\boldsymbol{U}(\boldsymbol{x}, t) - \boldsymbol{V}\right)\delta\left(\boldsymbol{\Phi}(\boldsymbol{x}, t) - \boldsymbol{\psi}\right) \equiv \prod_{i=1}^{3}\delta\left(U_i(\boldsymbol{x}, t) - V_i\right)\prod_{m=1}^{M+1}\delta\left(\Phi_m(\boldsymbol{x}, t) - \psi_m\right) \tag{29}$$

Its marginal FG-PDF for scalars is

$$f'_\Phi(\boldsymbol{\psi}; \boldsymbol{x}, t) \equiv \delta\left(\boldsymbol{\Phi}(\boldsymbol{x}, t) - \boldsymbol{\psi}\right) \equiv \prod_{m=1}^{M+1}\delta\left(\Phi_m(\boldsymbol{x}, t) - \psi_m\right) \tag{30}$$

where δ denotes the delta function, $\boldsymbol{U}(\boldsymbol{x},t)$ is the turbulent (random) velocity vector (U_1, U_2, U_3), $\boldsymbol{\Phi}(\boldsymbol{x},t)$ is the turbulent (random) scalar array $\left(\Phi_1, \Phi_2, \cdots, \Phi_M, \Phi_{M+1}\right)$, for example, M species mass fractions and one internal energy $\Phi_{M+1} = e$; the $\boldsymbol{x},t$ denote the physical space variable (x_1, x_2, x_3) and time t, $\boldsymbol{V} \equiv (V_1, V_2, V_3)$ and $\boldsymbol{\psi} \equiv (\psi_1, \psi_2, \cdots, \psi_M, \psi_{M+1})$ are the sample space variables for $\boldsymbol{U}(\boldsymbol{x},t)$ and $\boldsymbol{\Phi}(\boldsymbol{x},t)$, respectively.

3.1.2 Scalar APDF $F_\Phi(\boldsymbol{\psi}; \boldsymbol{x}, t)$

We define the following ensemble averaged density weighted fine-grained probability density function for scalars:

$$F_\Phi(\boldsymbol{\psi}; \boldsymbol{x}, t) \equiv \lim_{N\to\infty} \frac{1}{N} \sum_{n=1}^{N} \rho^{(n)}(\boldsymbol{x}, t)\, \delta\left(\boldsymbol{\Phi}^{(n)}(\boldsymbol{x}, t) - \boldsymbol{\psi}\right) \tag{31}$$

Obviously, the scalar APDF, $F_\Phi(\boldsymbol{\psi}; \boldsymbol{x}, t)$, is no longer a random quantity. And it satisfies the following "normalization" property:

$$\int_{-\infty}^{\infty} F_\Phi(\boldsymbol{\psi}; \boldsymbol{x}, t)\, d\boldsymbol{\psi} = \int_{-\infty}^{\infty} \lim_{N\to\infty} \frac{1}{N} \sum_{n=1}^{N} \rho^{(n)}(\boldsymbol{x}, t)\, \delta\left(\boldsymbol{\Phi}^{(n)}(\boldsymbol{x}, t) - \boldsymbol{\psi}\right) d\boldsymbol{\psi} = \lim_{N\to\infty} \frac{1}{N} \sum_{n=1}^{N} \rho^{(n)}(\boldsymbol{x}, t) = \overline{\rho} \tag{32}$$

Note that here $\int_{-\infty}^{\infty}$ means that the integration is over the entire domain of the sample space $\boldsymbol{\psi}$.

3.1.3 Relationship Between Scalar APDF and Averaged Turbulent Variables

With the definition of scalar APDF described in Equation (31), we can exactly deduce the averaged scalar turbulent variables that are defined in Equations (1) and (2). For example,

$$\begin{aligned}
\int_{-\infty}^{+\infty} \boldsymbol{\psi}\, F_\Phi(\boldsymbol{\psi}; \boldsymbol{x}, t)\, d\boldsymbol{\psi} &= \int_{-\infty}^{+\infty} \boldsymbol{\psi} \left(\lim_{N\to\infty} \frac{1}{N} \sum_{n=1}^{N} \rho^{(n)}(\boldsymbol{x}, t)\, \delta\left(\boldsymbol{\Phi}(\boldsymbol{x}, t) - \boldsymbol{\psi}\right) \right) d\boldsymbol{\psi} \\
&= \int_{-\infty}^{+\infty} \left(\lim_{N\to\infty} \frac{1}{N} \sum_{n=1}^{N} \rho^{(n)}(\boldsymbol{x}, t)\, \boldsymbol{\Phi}(\boldsymbol{x}, t)\, \delta\left(\boldsymbol{\Phi}(\boldsymbol{x}, t) - \boldsymbol{\psi}\right) \right) d\boldsymbol{\psi} \\
&= \lim_{N\to\infty} \frac{1}{N} \sum_{n=1}^{N} \rho^{(n)}(\boldsymbol{x}, t)\, \boldsymbol{\Phi}(\boldsymbol{x}, t) \\
&= \overline{\rho \boldsymbol{\Phi}} = \overline{\rho}(\boldsymbol{x}, t)\, \widetilde{\boldsymbol{\Phi}}(\boldsymbol{x}, t)
\end{aligned} \tag{33}$$

Equation (33) denotes that the left hand side is an operation $\langle \boldsymbol{\Phi} \rangle$ that defines the density weighed turbulent mean variable $\overline{\rho \boldsymbol{\Phi}}$:

$$\langle \boldsymbol{\Phi} \rangle \equiv \int_{-\infty}^{+\infty} \boldsymbol{\psi}\, F_\Phi(\boldsymbol{\psi}; \boldsymbol{x}, t)\, d\boldsymbol{\psi} = \overline{\rho}(\boldsymbol{x}, t)\, \widetilde{\boldsymbol{\Phi}}(\boldsymbol{x}, t) \tag{34}$$

For a function $W(\boldsymbol{\Phi}(\boldsymbol{x}, t))$, it is easy to verify that

$$\langle W(\boldsymbol{\Phi}) \rangle = \int_{-\infty}^{+\infty} W(\boldsymbol{\psi})\, F_\Phi(\boldsymbol{\psi}; \boldsymbol{x}, t)\, d\boldsymbol{\psi} = \overline{\rho}(\boldsymbol{x}, t)\, \widetilde{W}(\boldsymbol{\Phi}(\boldsymbol{x}, t)) \tag{35}$$

Furthermore, we may consider the derivatives $\nabla\boldsymbol{\Phi}$ as a new random quantity and legitimately write

$$\langle \nabla\boldsymbol{\Phi} \rangle = \overline{\rho}\, \widetilde{\nabla\boldsymbol{\Phi}} \tag{36}$$

However, because of the variable density, the "operation" $\langle\ \rangle$ does not have the differential commute property, i.e.,

$$\langle \nabla \boldsymbol{\Phi} \rangle \neq \nabla \langle \boldsymbol{\Phi} \rangle \tag{37}$$

because $\overline{\rho}\,\widetilde{\nabla \boldsymbol{\Phi}} \neq \nabla\left(\overline{\rho}\widetilde{\boldsymbol{\Phi}}\right)$.

We can also write the density weighted mean $\langle U_j \Phi_i \rangle$ for the joint velocity and scalar variables as

$$\langle U_j \Phi_i \rangle = \int_{-\infty}^{+\infty} V_j\, \psi_i\, F_{U,\Phi}(\boldsymbol{V}, \boldsymbol{\psi}; \boldsymbol{x}, t)\, d\boldsymbol{V} d\boldsymbol{\psi} = \overline{\rho}(\boldsymbol{x}, t)\widetilde{U_j \Phi_i}(\boldsymbol{x}, t) \tag{38}$$

where, $F_{U,\Phi}(\boldsymbol{V}, \boldsymbol{\psi}; \boldsymbol{x}, t)$ is the joint APDF defined as

$$F_{U,\Phi}(\boldsymbol{V}, \boldsymbol{\psi}; \boldsymbol{x}, t) = \lim_{N\to\infty} \frac{1}{N} \sum_{n=1}^{N} \rho^{(n)}(\boldsymbol{x}, t)\, \delta\left(\boldsymbol{U}^{(n)}(\boldsymbol{x}, t) - \boldsymbol{V}\right) \delta\left(\boldsymbol{\Phi}^{(n)}(\boldsymbol{x}, t) - \boldsymbol{\psi}\right) \tag{39}$$

which also satisfies the normalization property:

$$\int_{-\infty}^{\infty} \int_{-\infty}^{\infty} F_{U,\Phi}(\boldsymbol{V}, \boldsymbol{\psi}; \boldsymbol{x}, t)\, d\boldsymbol{V} d\boldsymbol{\psi} = \lim_{N\to\infty} \frac{1}{N} \sum_{n=1}^{N} \rho^{(n)}(\boldsymbol{x}, t) = \overline{\rho} \tag{40}$$

3.1.4 Joint APDF, $F_{U,\Phi}(\boldsymbol{V}, \boldsymbol{\psi}; \boldsymbol{x}, t)$ and Its Conditional APDF $F_{U|\Phi}(\boldsymbol{V}|\boldsymbol{\psi}; \boldsymbol{x}, t)$

From Equation (39), we may follow Reference 1 to define a "conditional" APDF on the condition $\boldsymbol{\Phi} = \boldsymbol{\psi}$ as

$$F_{U|\Phi}(\boldsymbol{V}|\boldsymbol{\psi}; \boldsymbol{x}, t) \equiv \frac{F_{U,\Phi}(\boldsymbol{V}, \boldsymbol{\psi}; \boldsymbol{x}, t)}{F_{\Phi}(\boldsymbol{\psi}; \boldsymbol{x}, t)} \tag{41}$$

and the "conditional mean" as

$$\begin{aligned} \langle \boldsymbol{U}(\boldsymbol{x}, t)|\boldsymbol{\psi} \rangle &\equiv \int_{-\infty}^{+\infty} \boldsymbol{V}\, F_{U|\Phi}(\boldsymbol{V}|\boldsymbol{\psi}; \boldsymbol{x}, t)\, d\boldsymbol{V} = \frac{1}{F_{\Phi}(\boldsymbol{\psi}; \boldsymbol{x}, t)} \int_{-\infty}^{+\infty} \boldsymbol{V}\, F_{U,\Phi}(\boldsymbol{V}, \boldsymbol{\psi}; \boldsymbol{x}, t)\, d\boldsymbol{V} \\ &= \frac{1}{F_{\Phi}} \int_{-\infty}^{+\infty} \boldsymbol{V} \left(\lim_{N\to\infty} \frac{1}{N} \sum_{n=1}^{N} \rho^{(n)}(\boldsymbol{x}, t)\, \delta\left(\boldsymbol{U}^{(n)}(\boldsymbol{x}, t) - \boldsymbol{V}\right) \delta\left(\boldsymbol{\Phi}^{(n)}(\boldsymbol{x}, t) - \boldsymbol{\psi}\right) \right) d\boldsymbol{V} \\ &= \frac{1}{F_{\Phi}} \lim_{N\to\infty} \frac{1}{N} \sum_{n=1}^{N} \rho^{(n)}(\boldsymbol{x}, t)\, \boldsymbol{U}^{(n)}\, \delta\left(\boldsymbol{\Phi}^{(n)}(\boldsymbol{x}, t) - \boldsymbol{\psi}\right) \end{aligned} \tag{42}$$

Then we have

$$\lim_{N\to\infty} \frac{1}{N} \sum_{n=1}^{N} \rho^{(n)}(\boldsymbol{x}, t)\, \boldsymbol{U}^{(n)}\, \delta\left(\boldsymbol{\Phi}^{(n)}(\boldsymbol{x}, t) - \boldsymbol{\psi}\right) = \int_{-\infty}^{+\infty} \boldsymbol{V}\, F_{U,\Phi}(\boldsymbol{V}, \boldsymbol{\psi}; \boldsymbol{x}, t)\, d\boldsymbol{V} = F_{\Phi} \cdot \langle \boldsymbol{U}(\boldsymbol{x}, t)|\boldsymbol{\psi} \rangle \tag{43}$$

And the "complete" mean should be

$$\int_{-\infty}^{+\infty}\left(\left\langle \boldsymbol{U}(\boldsymbol{x},t)\middle|\boldsymbol{\psi}\right\rangle\cdot F_{\Phi}\right)d\boldsymbol{\psi}$$
$$=\int_{-\infty}^{+\infty}\int_{-\infty}^{+\infty}\boldsymbol{V}\lim_{N\to\infty}\frac{1}{N}\sum_{n=1}^{N}\rho^{(n)}(\boldsymbol{x},t)\delta\left(\boldsymbol{U}^{(n)}(\boldsymbol{x},t)-\boldsymbol{V}\right)\delta\left(\boldsymbol{\Phi}^{(n)}(\boldsymbol{x},t)-\boldsymbol{\psi}\right)d\boldsymbol{V}d\boldsymbol{\psi} \tag{44}$$
$$=\lim_{N\to\infty}\frac{1}{N}\sum_{n=1}^{N}\rho^{(n)}(\boldsymbol{x},t)\boldsymbol{U}^{(n)}(\boldsymbol{x},t)=\overline{\rho}(\boldsymbol{x},t)\widetilde{\boldsymbol{U}}(\boldsymbol{x},t)$$

Equation (43) can be extended to any other turbulent quantities, for example, $\nabla\boldsymbol{\Phi}$, $S_i(\boldsymbol{\Phi})$:

$$\begin{aligned}&\lim_{N\to\infty}\frac{1}{N}\sum_{n=1}^{N}\rho^{(n)}\left(\nabla\boldsymbol{\Phi}\right)^{(n)}\delta\left(\boldsymbol{\Phi}^{(n)}(\boldsymbol{x},t)-\boldsymbol{\psi}\right)=F_{\Phi}\cdot\left\langle\nabla\boldsymbol{\Phi}\middle|\boldsymbol{\psi}\right\rangle\\&\lim_{N\to\infty}\frac{1}{N}\sum_{n=1}^{N}\rho^{(n)}S_i{}^{(n)}\delta\left(\boldsymbol{\Phi}^{(n)}(\boldsymbol{x},t)-\boldsymbol{\psi}\right)=F_{\Phi}\cdot\left\langle S_i(\boldsymbol{\Phi})\middle|\boldsymbol{\psi}\right\rangle=F_{\Phi}\cdot S_i(\boldsymbol{\psi})\end{aligned} \tag{45}$$

where $\nabla\boldsymbol{\Phi}$ is viewed as a new random variable in addition to $\boldsymbol{\Phi}$.

3.2 Transport Equation for Scalar APDF $F_{\Phi}(\boldsymbol{\psi};\boldsymbol{x},t)$

We may derive the transport equation for scalar APDF from Equations (16) and (17) as follows: first, we write the terms on the left hand side of Equation (17) as

$$\frac{\partial\overline{\rho}\,\widetilde{\Phi}_m}{\partial t}=\frac{\partial}{\partial t}\int_{-\infty}^{\infty}\psi_m F_{\Phi}\,d\boldsymbol{\psi}=\int_{-\infty}^{\infty}\psi_m\frac{\partial F_{\Phi}}{\partial t}d\boldsymbol{\psi} \tag{46}$$

$$\frac{\partial\overline{\rho}\,\widetilde{U_i\Phi_m}}{\partial x_i}=\frac{\partial}{\partial x_i}\int_{-\infty}^{\infty}\int_{-\infty}^{\infty}V_i\,\psi_m F_{U,\Phi}\,d\boldsymbol{V}d\boldsymbol{\psi}=\begin{cases}\displaystyle\int_{-\infty}^{\infty}\int_{-\infty}^{\infty}\psi_m\left(V_i\frac{\partial}{\partial x_i}F_{U,\Phi}\right)d\boldsymbol{V}\,d\boldsymbol{\psi}\\ \text{or}\\ \displaystyle\int_{-\infty}^{\infty}\psi_m\left(\frac{\partial}{\partial x_i}\left(F_{\Phi}\cdot\left\langle U_i\middle|\boldsymbol{\psi}\right\rangle_L\right)\right)d\boldsymbol{\psi}\end{cases} \tag{47}$$

Then, the terms on the right hand side of Equation (17) can be written as

$$\frac{\partial}{\partial x_i}\left(\Gamma^{(m)}\frac{\partial\overline{\rho}\,\widetilde{\Phi}_m}{\partial x_i}\right)=\frac{\partial}{\partial x_i}\left(\Gamma^{(m)}\frac{\partial}{\partial x_i}\int_{-\infty}^{\infty}\psi_m F_{\Phi}\,d\boldsymbol{\psi}\right)=\begin{cases}\displaystyle\int_{-\infty}^{\infty}\psi_m\frac{\partial}{\partial x_i}\left(\Gamma^{(m)}\frac{\partial F_{\Phi}}{\partial x_i}\right)d\boldsymbol{\psi}\\ \text{or}\\ \displaystyle-\int_{-\infty}^{\infty}\psi_m\frac{\partial}{\partial x_i}\left(\Gamma^{(m)}\frac{\partial^2\psi_k F_{\Phi}}{\partial\psi_k\partial x_i}\right)d\boldsymbol{\psi}\end{cases} \tag{48}$$

$$\overline{\rho}\,\widetilde{S}_m=\int_{-\infty}^{\infty}S_m(\boldsymbol{\psi})F_{\Phi}d\boldsymbol{\psi}=-\int_{-\infty}^{\infty}\psi_m\frac{\partial\left(S_k F_{\Phi}\right)}{\partial\psi_k}d\boldsymbol{\psi} \tag{49}$$

Where in Equations (48) and (49) we have applied the integration by parts and the following zero integration:

$$\int_{-\infty}^{\infty} \frac{\partial}{\partial \boldsymbol{\psi}} \left[A(\boldsymbol{\psi}) \cdot F_{\Phi} \right] d\boldsymbol{\psi} = 0, \quad \text{if a finite mean } \langle A \rangle \text{ exists.} \tag{50}$$

Collecting all the integrand terms, and let the sum be zero (we refer this as the conservation condition, which is in general a sufficient but not necessary condition, Ref. 16), we obtain

$$\frac{\partial F_{\Phi}}{\partial t} + \frac{\partial \left(F_{\Phi} \cdot \langle U_i | \boldsymbol{\psi} \rangle \right)}{\partial x_i} = \left\{ \frac{\partial}{\partial x_i} \left(\Gamma^{(m)} \frac{\partial F_{\Phi}}{\partial x_i} \right) - \frac{\partial}{\partial \psi_k} \left[F_{\Phi} \cdot S_k(\boldsymbol{\psi}) \right] \right\}, \quad k = 1, 2, \cdots, M+1$$

or

$$\frac{\partial F_{\Phi}}{\partial t} + \frac{\partial \left(F_{\Phi} \cdot \langle U_i | \boldsymbol{\psi} \rangle \right)}{\partial x_i} = -\frac{\partial}{\partial \psi_k} \left\{ \frac{\partial}{\partial x_i} \left(\Gamma^{(m)} \psi_k \frac{\partial F_{\Phi}}{\partial x_i} \right) + F_{\Phi} \cdot S_k(\boldsymbol{\psi}) \right\}, \quad k = 1, 2, \cdots, M+1 \tag{51}$$

This equation also includes the equation of internal energy when $S_{M+1}(\boldsymbol{\psi}) = 0$ and other source terms in Equation (16) are neglected. Unlike the case of the joint APDF $F_{U,\Phi}$, for the marginal F_{Φ}, the convection term is not closed because of the conditional mean $\langle U_i | \boldsymbol{\psi} \rangle$. Then, this critically important term, corresponding to $\overline{\rho} \widetilde{U_i \Phi}_m$ in Equation (17), must be carefully modeled while the less important molecular diffusion term remains in the closed form. In addition, we noticed that the equally important chemistry source term $\overline{\rho} \widetilde{S_m(\boldsymbol{\Phi})}$ in Equation (17), which involves complex processes of turbulence-chemistry interaction, is closed in the scalar APDF equation, i.e., no need of modeling. This direct calculation of turbulence-chemistry interaction is one of the unique features of the PDF methodology.

3.3 Nonlinear Model for Scalar Fluxes

The convection term in Equation (51) contains the term $F_{\Phi} \cdot \langle U_i | \boldsymbol{\psi} \rangle$, which must be modeled. We may start from a nonlinear model, Equation (26), for the term $\overline{\rho} \widetilde{U_i \Phi_m}$:

$$\overline{\rho} \widetilde{U_i \Phi_m} = \overline{\rho} \widetilde{U}_i \widetilde{\Phi}_m - \Gamma_T^{(m)} \frac{\partial \overline{\rho} \widetilde{\Phi}_m}{\partial x_i} - \Gamma_T^{(m)} \frac{k}{\varepsilon} \left(c_1 \widetilde{S}_{ij} + c_2 \widetilde{\Omega}_{ij} \right) \frac{\partial \overline{\rho} \widetilde{\Phi}_m}{\partial x_j} \tag{52}$$

This will lead to the following model by directly applying Equations (34) and (43):

$$F_{\Phi} \cdot \langle U_i | \boldsymbol{\psi} \rangle = \widetilde{U}_i F_{\Phi} - \left[\Gamma_T^{(m)} \frac{\partial F_{\Phi}}{\partial x_i} \right] + \frac{\partial}{\partial \psi_k} \left[\Gamma_T^{(m)} \frac{k}{\varepsilon} \left(c_1 \widetilde{S}_{ij} + c_2 \widetilde{\Omega}_{ij} \right) \psi_k \frac{\partial F_{\Phi}}{\partial x_j} \right]$$

or

$$F_{\Phi} \cdot \langle U_i | \boldsymbol{\psi} \rangle = \widetilde{U}_i F_{\Phi} + \frac{\partial}{\partial \psi_k} \left[\Gamma_T^{(m)} \psi_k \frac{\partial F_{\Phi}}{\partial x_i} \right] + \frac{\partial}{\partial \psi_k} \left[\Gamma_T^{(m)} \frac{k}{\varepsilon} \left(c_1 \widetilde{S}_{ij} + c_2 \widetilde{\Omega}_{ij} \right) \psi_k \frac{\partial F_{\Phi}}{\partial x_j} \right] \tag{53}$$

3.4 Summary

With the model given by Equation (53), the scalar APDF equation for $F_\Phi(\boldsymbol{\psi};\boldsymbol{x},t)$ can be written as

$$\frac{\partial F_\Phi}{\partial t}+\frac{\partial\left(\widetilde{U}_i F_\Phi\right)}{\partial x_i}=\left\{\frac{\partial}{\partial x_i}\left(\left(\Gamma^{(m)}+\Gamma_T^{(m)}\right)\frac{\partial F_\Phi}{\partial x_i}\right)\right\}-\frac{\partial}{\partial \psi_k}\left(F_\Phi\cdot S_k\left(\boldsymbol{\psi}\right)\right)$$
$$-\frac{\partial}{\partial \psi_k}\left\{\psi_k\frac{\partial}{\partial x_i}\left(\Gamma_T^{(m)}\frac{k}{\varepsilon}\left(c_1\widetilde{S}_{ij}+c_2\widetilde{\Omega}_{ij}\right)\frac{\partial F_\Phi}{\partial x_j}\right)\right\},\qquad k=1,2,\cdots,M+1 \tag{54}$$

It can be verified that the scalar APDF Equation (54) can exactly deduce the ensemble averaged Equation (17). However, the model described by this equation is by no means unique. In addition, the variables ($\widetilde{U}_i$, $\widetilde{S}_{ij}$ and $\widetilde{\Omega}_{ij}$) are considered to be available during the solution procedure of the scalar APDF equation. Furthermore, in order to apply the available stochastic solution procedure built in the NCC code, we further simplify the model term in Equation (54) as follows:

$$-\frac{\partial}{\partial \psi_k}\left\{\psi_k\frac{\partial}{\partial x_i}\left(\Gamma_T^{(m)}\frac{k}{\varepsilon}\left(c_1\widetilde{S}_{ij}+c_2\widetilde{\Omega}_{ij}\right)\frac{\partial F_\Phi}{\partial x_j}\right)\right\}=\frac{\partial}{\partial \psi_k}\left(\psi_k\frac{1}{\tau}F_\Phi\right) \tag{55}$$

where

$$\frac{1}{\tau}\equiv-\frac{1}{F_\Phi}\frac{\partial}{\partial x_i}\left(\Gamma_T^{(m)}\frac{k}{\varepsilon}\left(c_1\widetilde{S}_{ij}+c_2\widetilde{\Omega}_{ij}\right)\frac{\partial F_\Phi}{\partial x_j}\right)\approx\sqrt{\widetilde{S}_{ij}\widetilde{S}_{ij}+\widetilde{\Omega}_{ij}\widetilde{\Omega}_{ij}} \tag{56}$$

Equation (56) is a crude approximation based on the dimensional argument for a time scale, which is responsible for the diffusion of scalar APDF in the space ψ_k. We chose this time scale to be related to the rate of strain and rotation instead of its complex formulation. In order to prevent this time scale from being non-physically small during the simulation, we require that

$$\tau\geq\sqrt{\left(\nu+\nu_T\right)/\varepsilon} \tag{57}$$

because the right hand side of Equation (57) represents the smallest time scale of the simulated flow field.

4.0 Numerical Simulations of Single Element LDI Injector

The lean direct injection (LDI) injector is a liquid fuel injector developed to reduce aircraft emissions. Stable combustion is essentially completed within a short distance through rapid fuel and air mixing. This design also allows for many small fuel injectors integrated into modules facilitating different fuel staging strategies, such as the one shown in Figure 1. So far, experimental observations have not fully clarified the dynamics of the mixing and combustion processes occurring in these injectors, and numerical studies need to be conducted to achieve a better understanding of the underlying physics of the LDI combustor. Figure 2 shows the air swirler and the convergent-divergent nozzle of the single element injector. Figure 3 depicts the single element LDI combustor geometry and its computational domain. Five probes are dispatched along the centerline (Figure 4) to monitor the evolution of turbulent variables during the simulations. The numerical grid is formed using hexahedral elements and the total number of elements is about 862,000, which is a relatively coarse grid used in a previous RANS simulation (Ref. 17).

Figure 1.—Nine element LDI module.

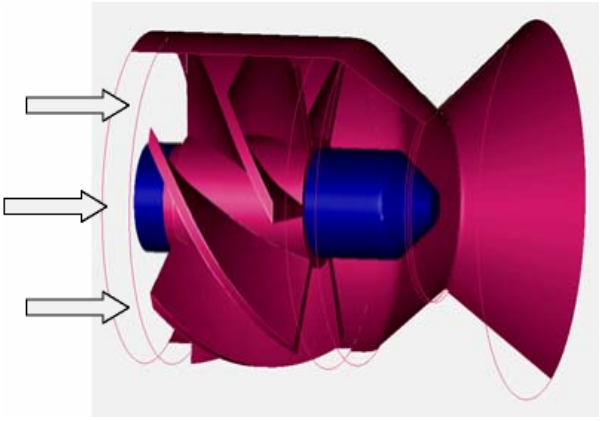

Figure 2.—Single element LDI injector.

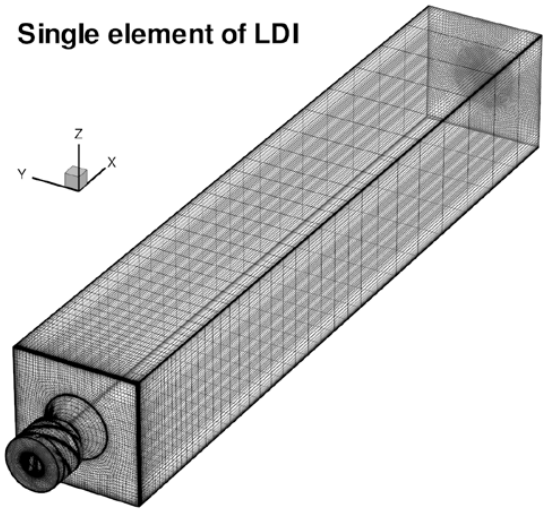

Figure 3.—Computational domain and grid spacing.

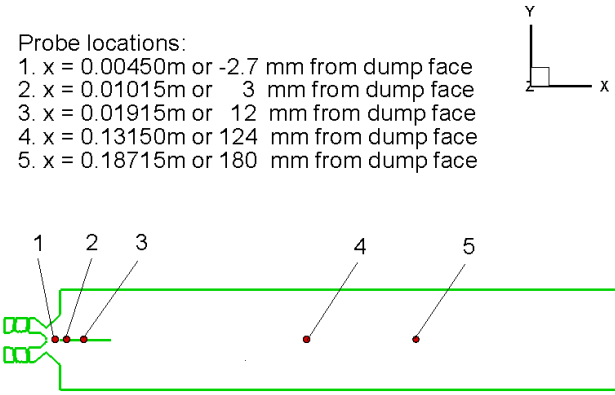

Figure 4.—Probes located on centerline.

In this study, the liquid fuel is Jet-A, and C12H23 is adopted as its surrogate, the fuel is injected at the throat of the nozzle, mixing with the swirling air that comes from the air swirlers which consists of six helical, axial vanes with downstream vane angles of 60°. A prescribed droplet-size distribution spray model is used. In Section 4.1, we present the results of steady simulations. We first carry out a steady RANS

simulation with a "laminar chemistry" model, in which the generation rate of compositions is determined by the mean turbulent variables, which is commonly considered as a very crude assumption or model for the chemistry-turbulence interaction. This simulation has been carried out up to 900,000 iterations. Then we start a new simulation using the solution of the abovementioned simulation at the iteration of 460,000 as the initial condition and invoking an Eulerian scalar PDF method, in which the compositions and internal energy will be determined by the scalar APDF equation while the flow field is still determined by the continuity and momentum equations of the averaged Navier-Stokes equations. Since the production rate of composition is in a closed form in the scalar APDF equation, it can be calculated without modeling. This new simulation is carried out up to 760,000 iterations. In Section 4.2, we present the results of unsteady simulations URANS to consider the strong unsteadiness of LDI flow, using both with and without scalar PDF method. The stochastic numerical procedures for solving scalar APDF equation and fuel spray equations are described in Reference 3 and adopted in the present simulations.

4.1 Results of RANS Simulations With and Without Invoking an Eulerian Scalar APDF

In this section we present results of steady simulations with and without invoking the scalar APDF equation. Figure 5 shows the general pictures of simulated spray reacting flow in a single element LDI injector by both methods. Most of the results will be presented side by side for comparisons. The main results are presented in terms of 1) the variations of velocity components and temperature with respect to the iteration at five probes along the centerline (see Figure 4), which indicate how much the simulated reacting flow is developed, 2) the centerline distributions of temperature and axial velocity, 3) the temperature and velocity profiles along Z axis at several downstream locations, 4) the center recirculation zone visualized by isosurface of zero axial velocity and the contour plots of various turbulent quantities in the center x-z plane. These profiles, isosurface and contour plots will provide the information about flow and flame structures of the simulated spray reacting flow. Some available experimental data (Ref. 18) are also plotted for comparison with the calculated results from the simulations.

4.1.1 Variation of Velocity and Temperature at Five Probes Along the Centerline

Figure 6 and Figure 7 are the recorded iteration histories of velocity components and temperature at the five probes during the course of the steady simulations for the last 150,000 iterations. These figures indicate that the RANS simulation with the scalar APDF equation has reached its "steady" solution even before 600,000 iterations, the last 150,000 iterations are used for checking if the solution can be sustained or not. However, the conventional RANS without PDF method has the difficulty to reach its steady state and continues to vary around its "mean" value, which is clearly shown in the last 150,000 iterations.

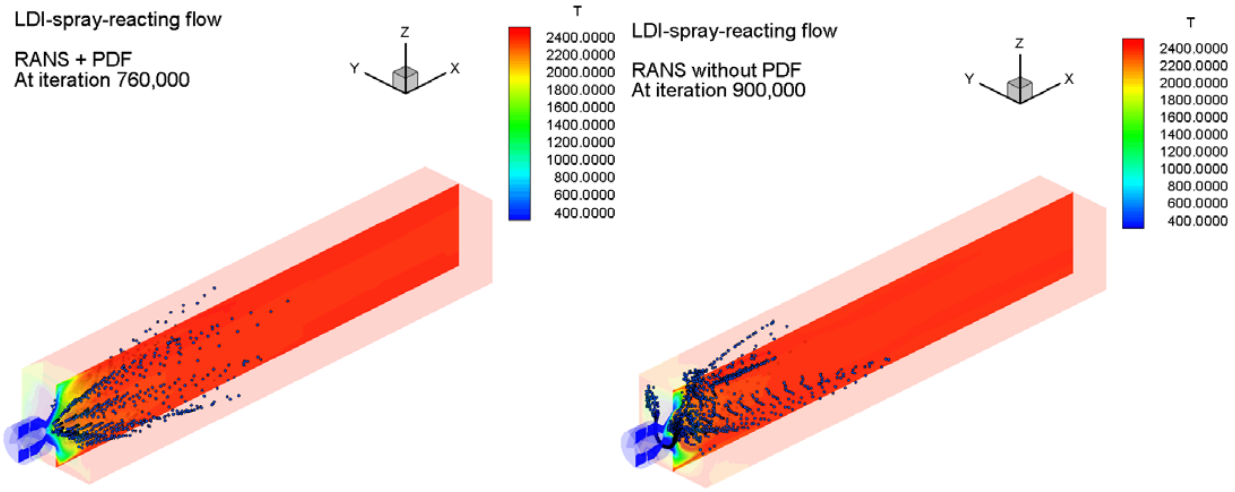

Figure 5.—Global pictures of spray reacting flow simulated with and without scalar PDF method.

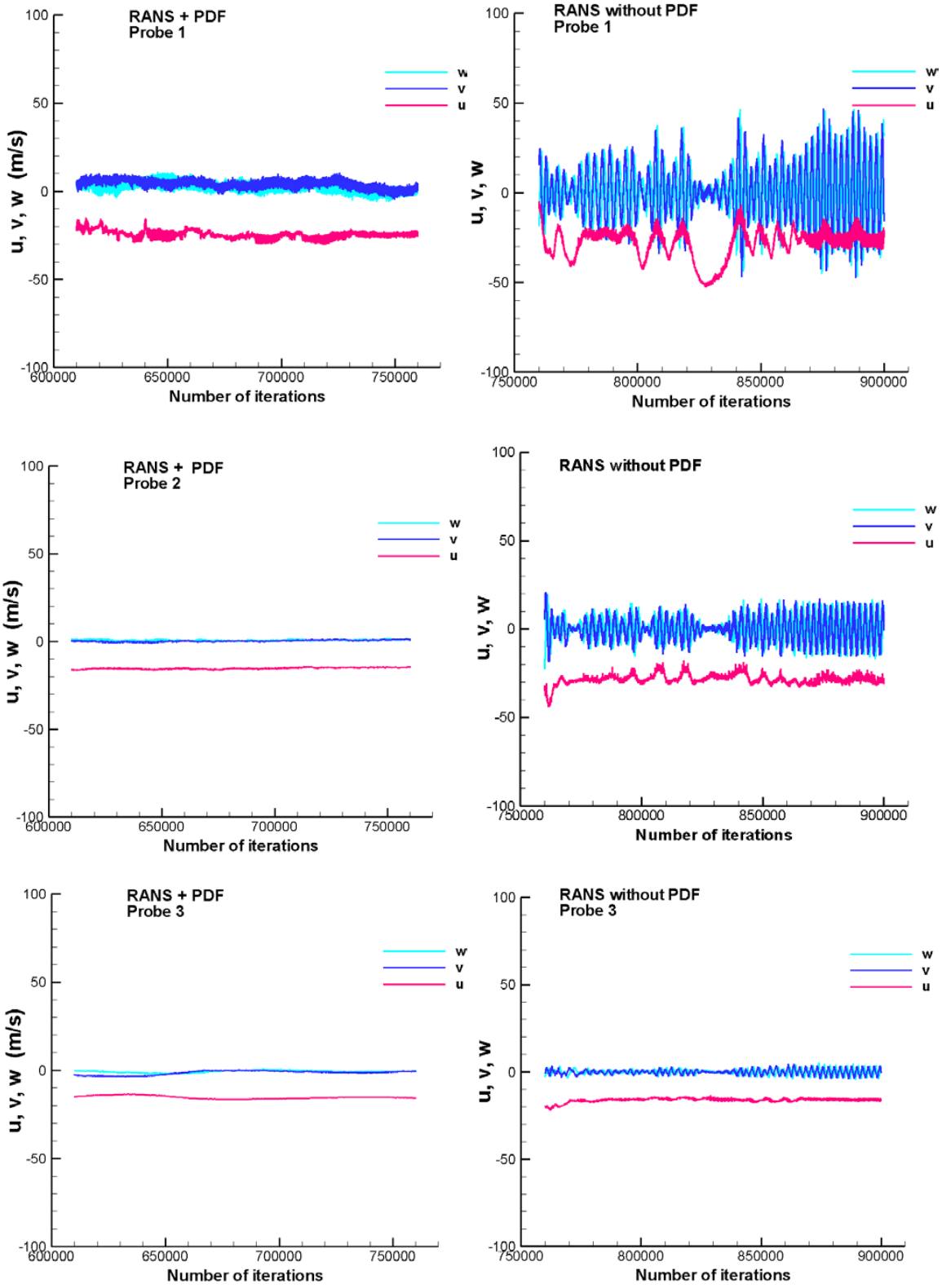

Figure 6.—Comparison of variations of simulated velocity components at 5 probes.

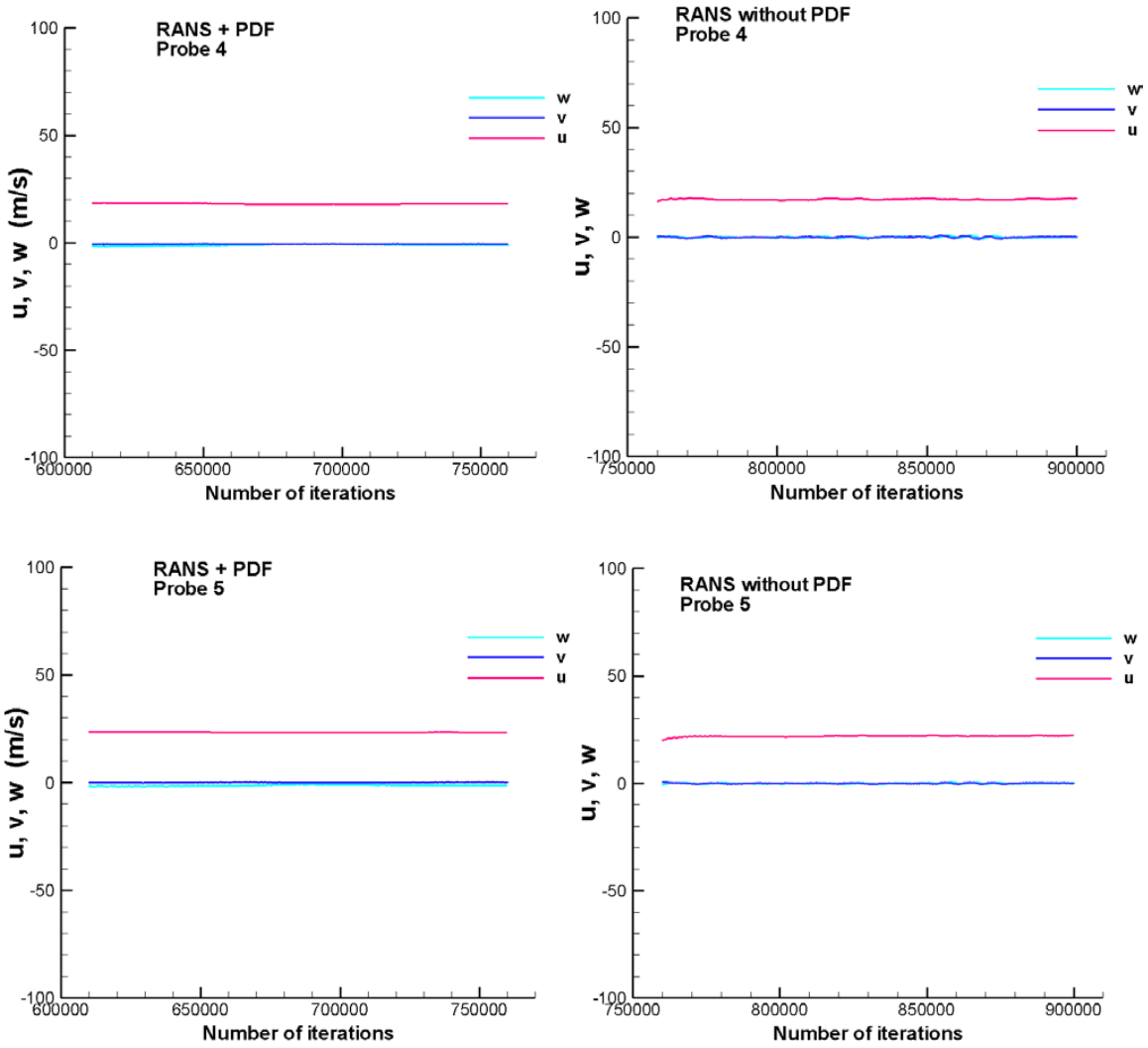

Figure 6.—Concluded.

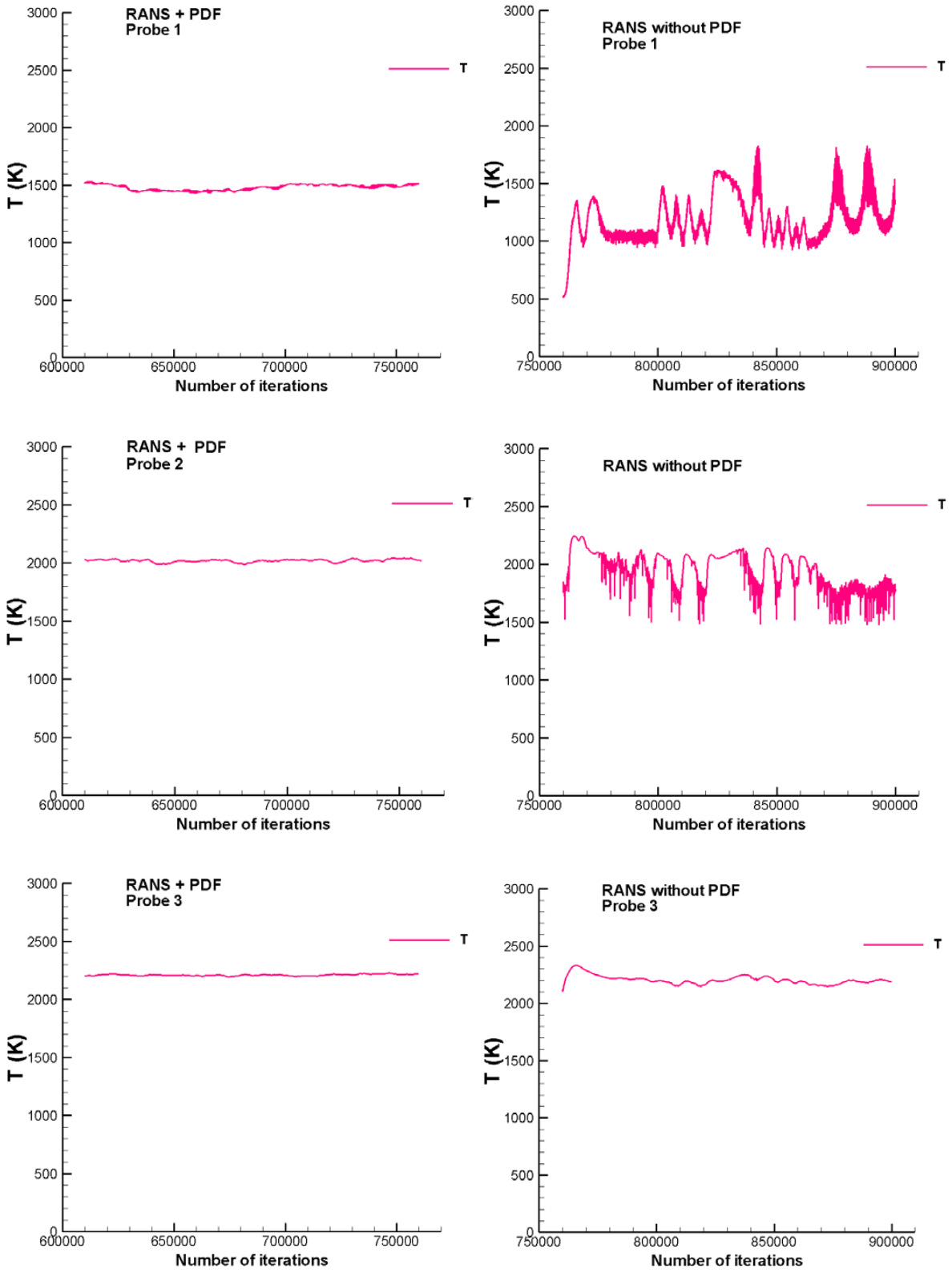

Figure 7.—Comparison of variations of simulated temperature at 5 probes.

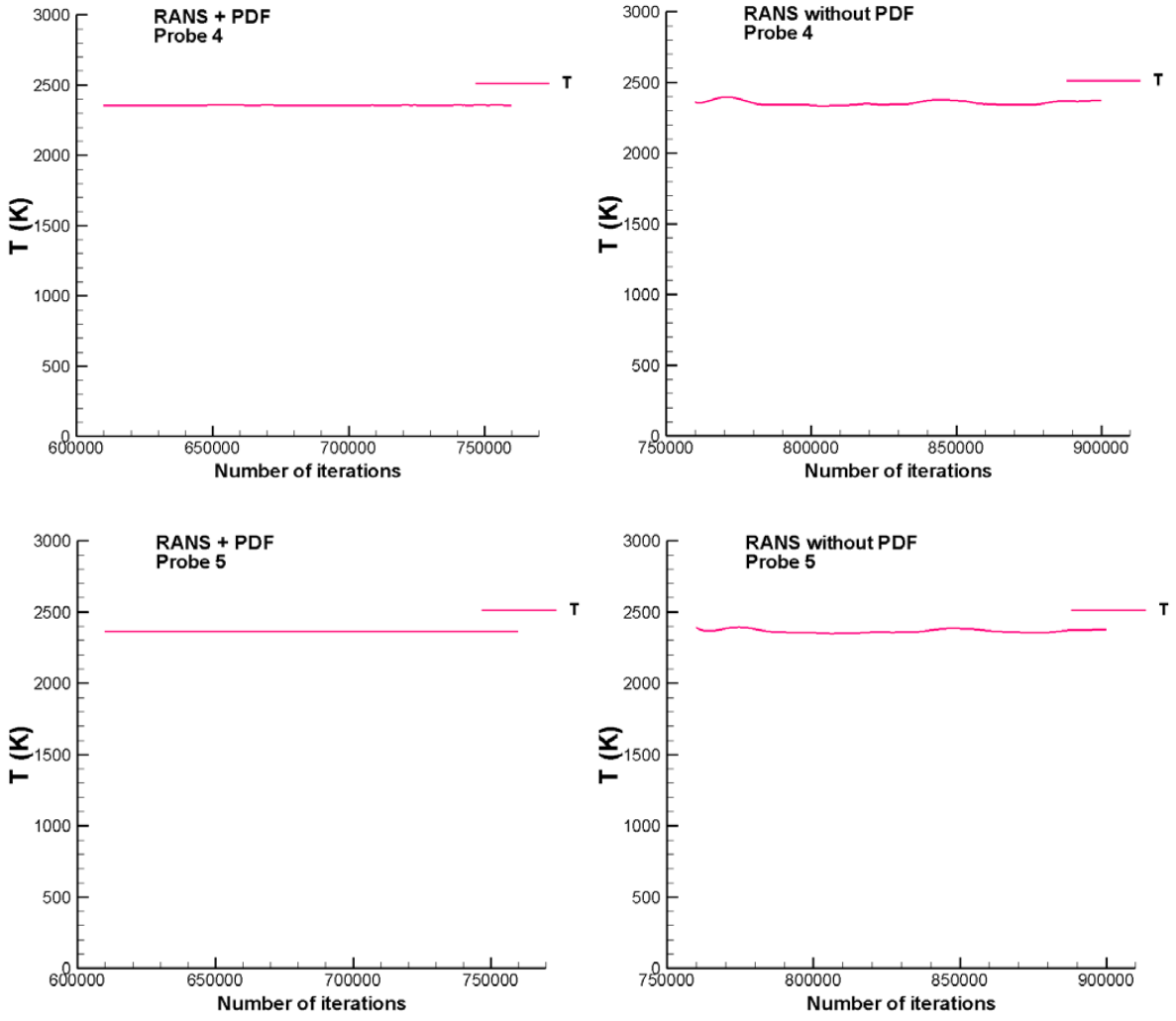

Figure 7.—Concluded.

4.1.2 Centerline Distributions of Mean Temperature and Axial Velocity

Figure 8 compares the centerline distribution of axial velocity with experimental data. The improvement in the nozzle region has been made by the PDF method. However, Figure 9 shows that the centerline distribution of temperature, comparing with the experimental data, is over predicted by the both methods in the region after the front face of dump combustor.

4.1.3 Mean Temperature and Velocity Profiles Along Z Axis at Downstream Locations

Temperature profiles along Z axis at ten downstream locations have been plotted. Here we only show four locations at x = 5, 10, 20 and 200 mm downstream of the front face of dump combustor. Comparing with the experimental data, Figure 10 clearly reveals the improvement made by the RAN simulation with the APDF equation. Similar situations are observed in the profiles of velocity components V and U along Z axis, shown in Figure 11 and Figure 12.

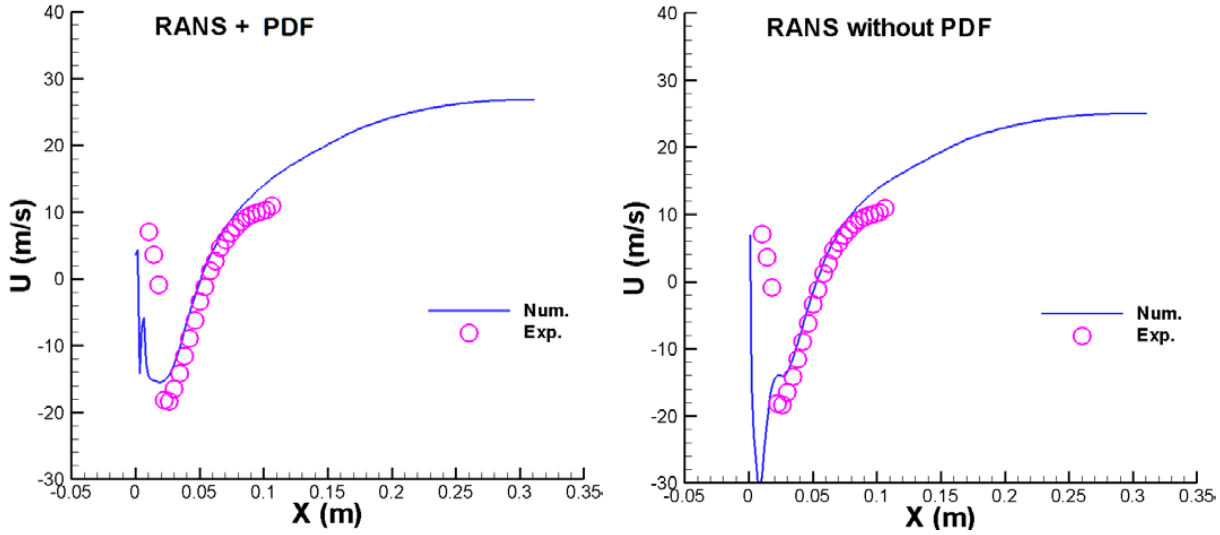

Figure 8.—Comparison of centerline distribution of axial velocity.

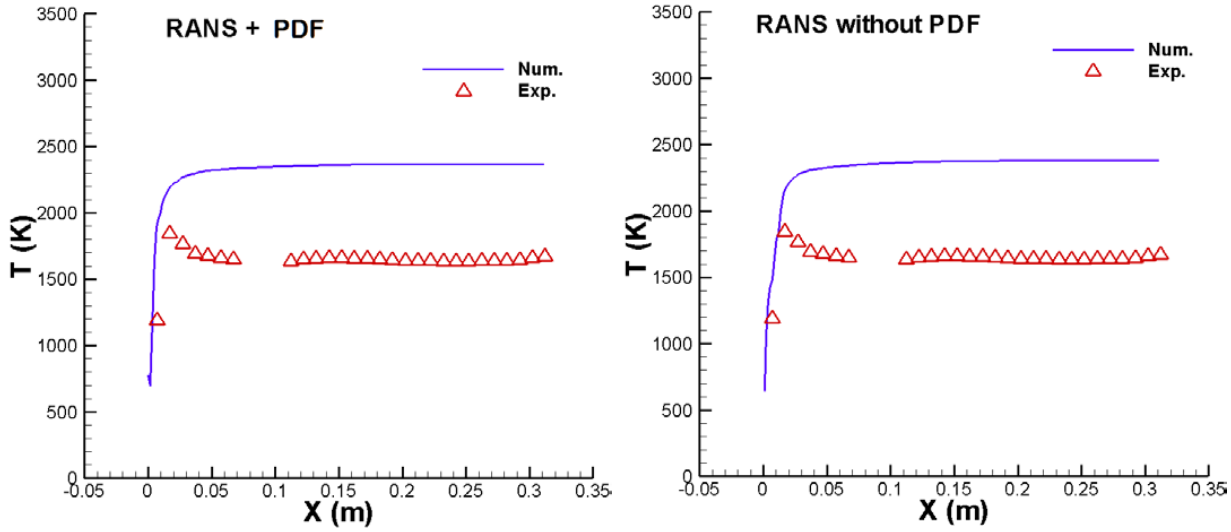

Figure 9.—Comparison of centerline distribution of temperature.

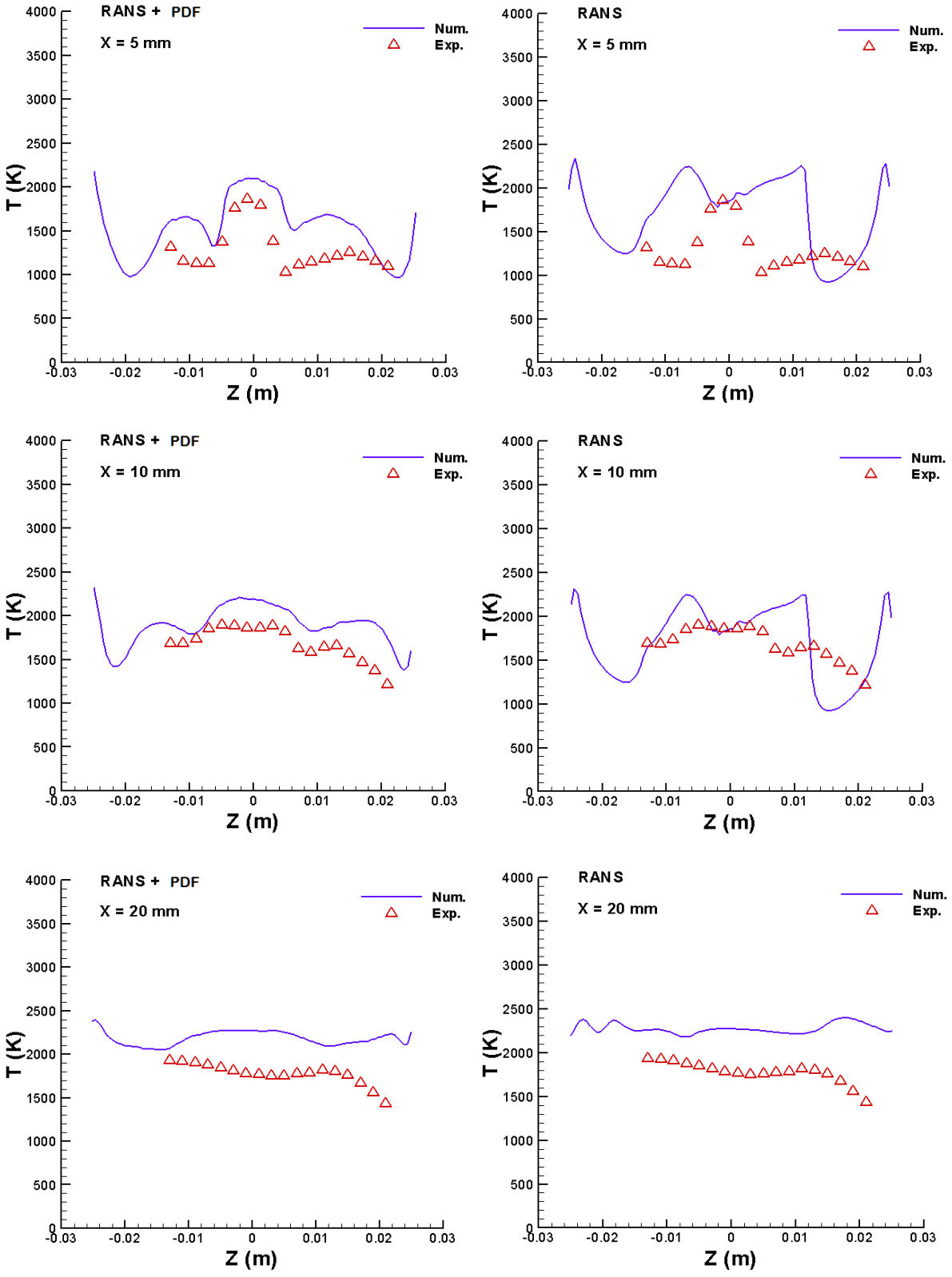

Figure 10.—Comparison of temperature distribution along Z axis at downstream locations.

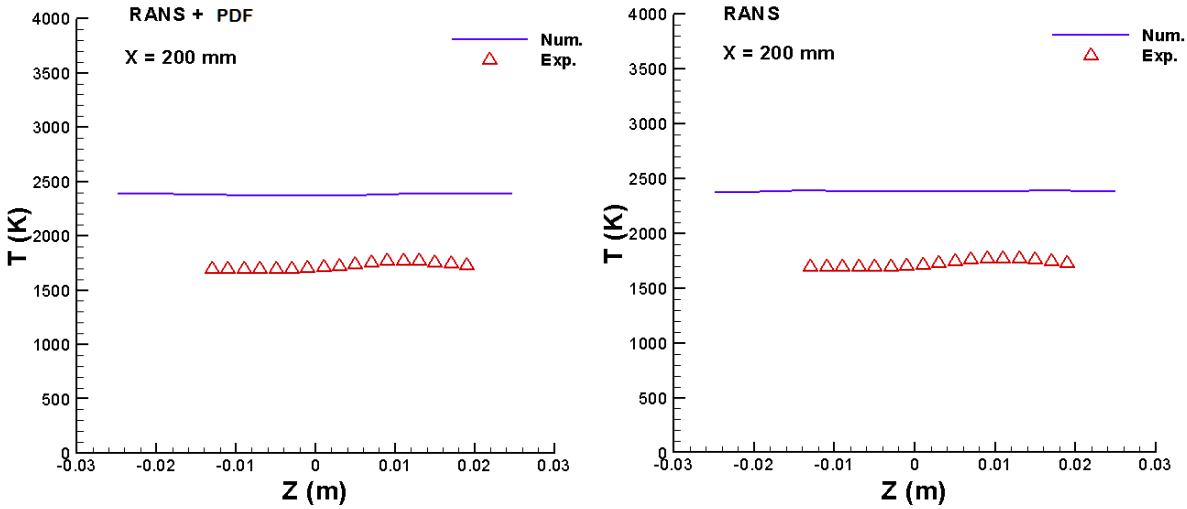

Figure 10.—Concluded.

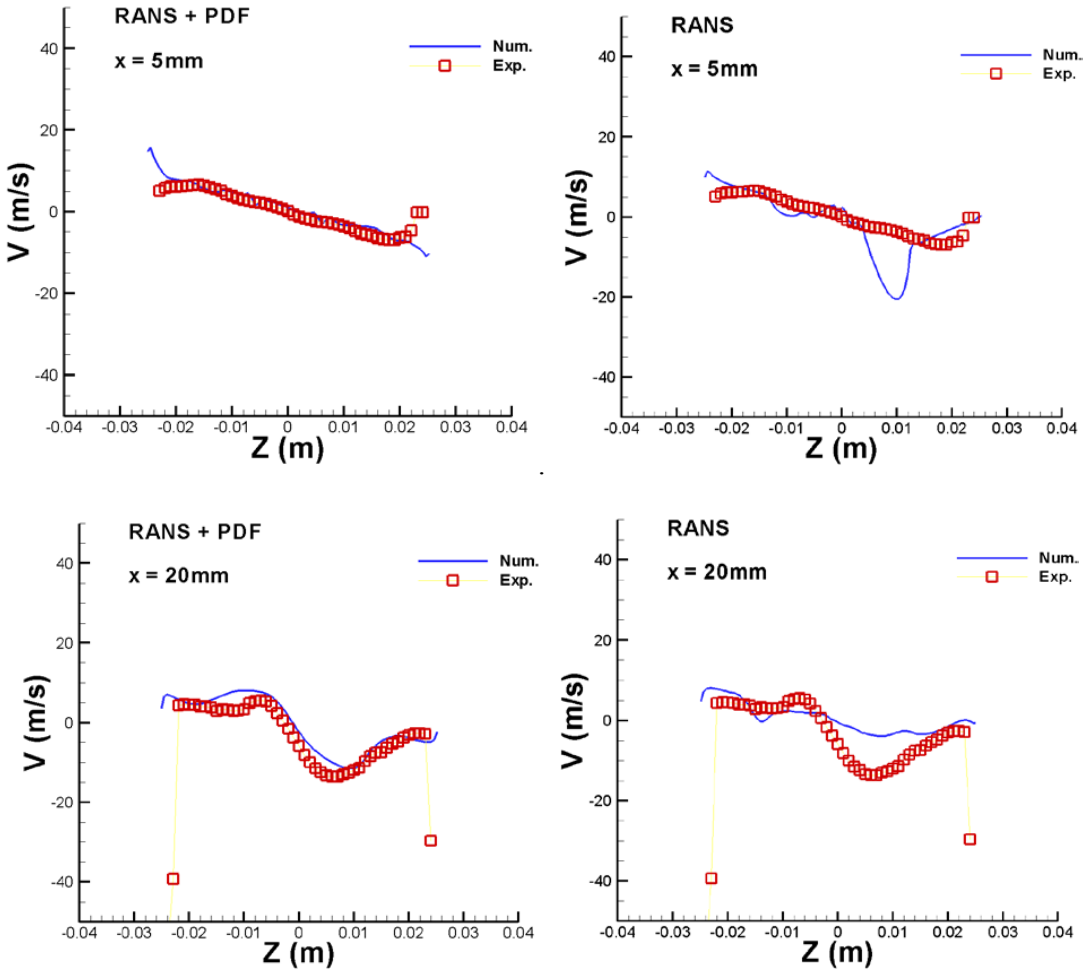

Figure 11.—Comparison of V distribution along Z axis at downstream locations.

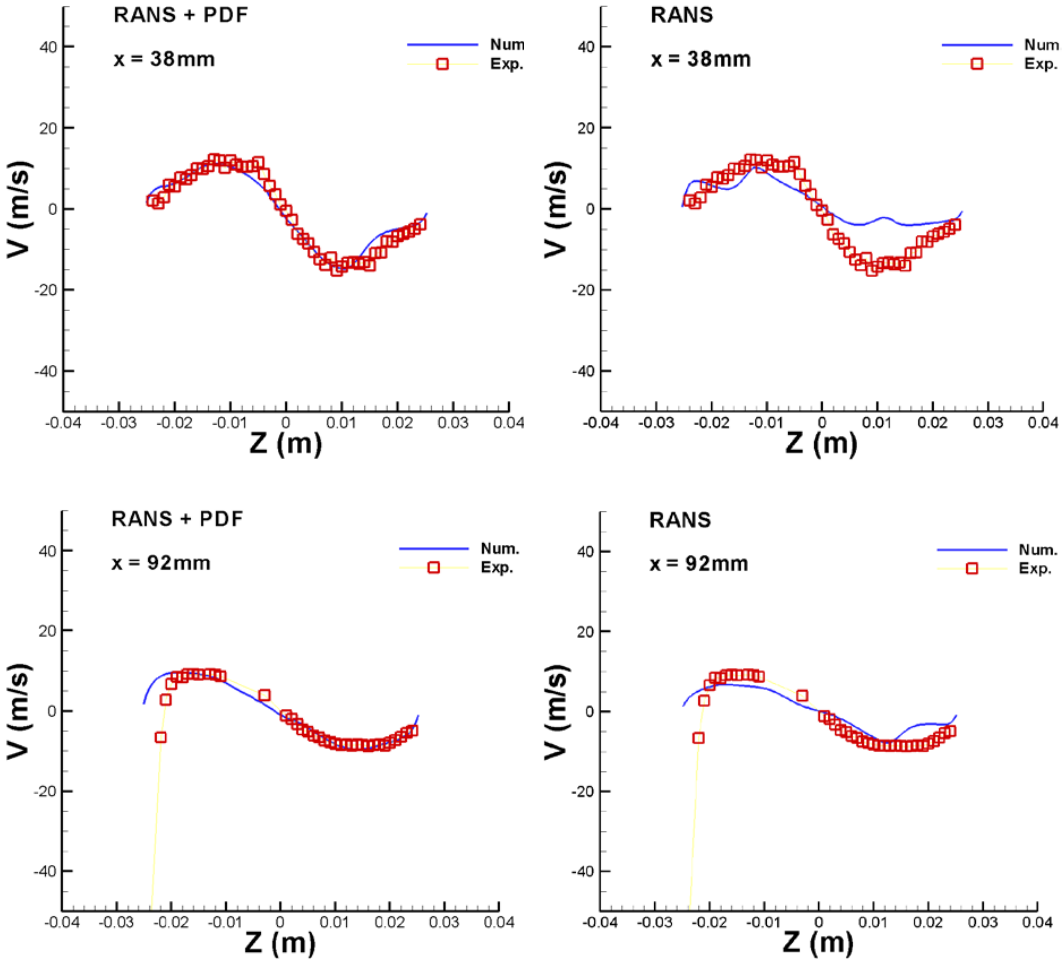

Figure 11.—Concluded.

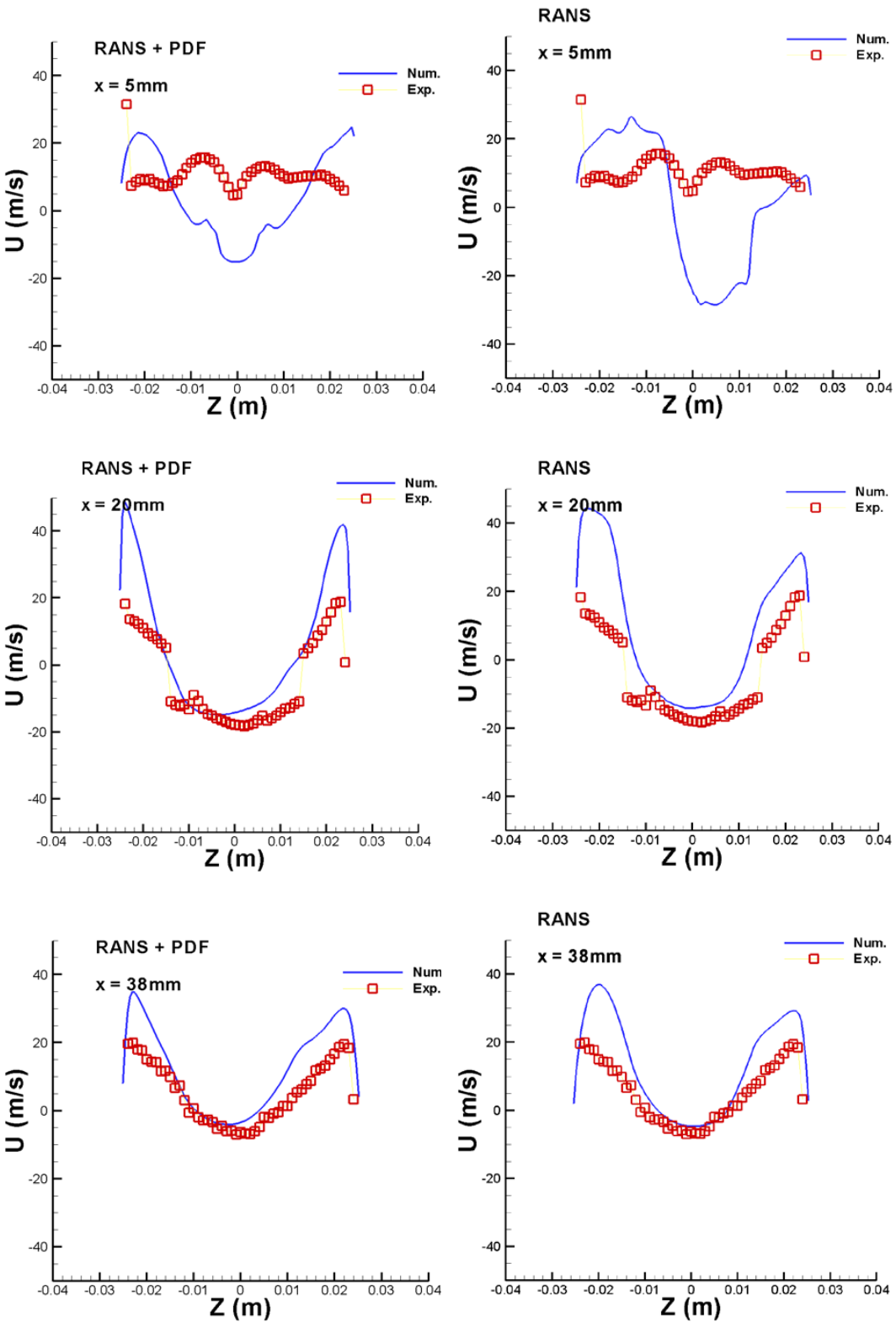

Figure 12.—Comparison of U distribution along Z axis at downstream locations.

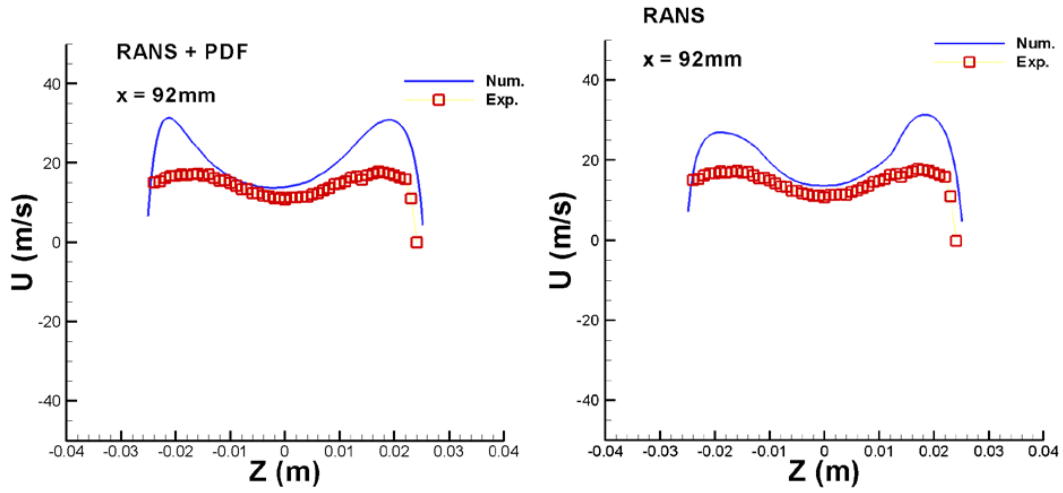

Figure 12.—Concluded.

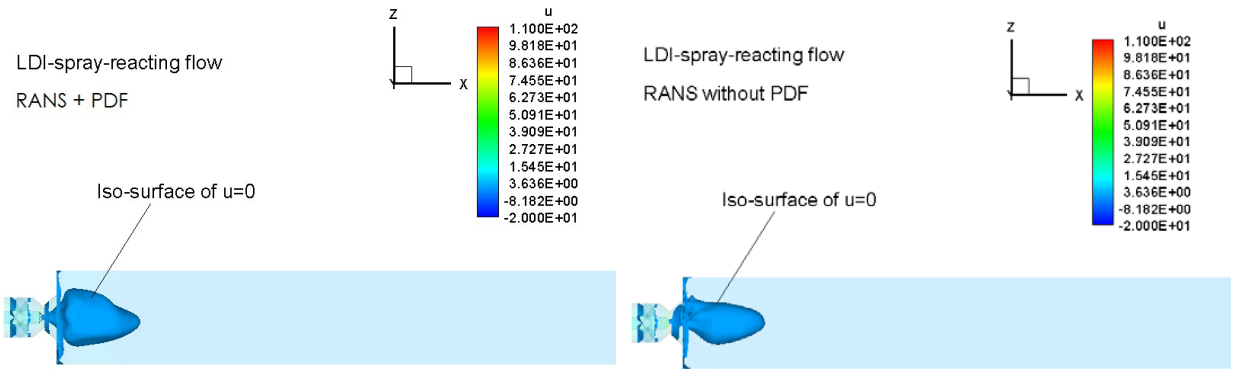

Figure 13.—Comparison of center recirculation zone.

4.1.4 Mean Flow Structure and Contour Plots of Variables in the Center x-z Plane

To reveal the simulated flow and flame structures, we have plotted the center recirculation zone visualized by the isosurface of zero axial velocity (see Figure 13), the contour plots of velocity components, temperature, turbulent kinetic energy, species mass fraction C12H23, O2 and CO2 are shown in Figure 14, Figure 15, and Figure 16. From these figures we observed that all the structures simulated by RANS with APDF equation are more symmetric than the ones from the RANS without PDF method. This trend of symmetry seems more lined up with the experimental observation.

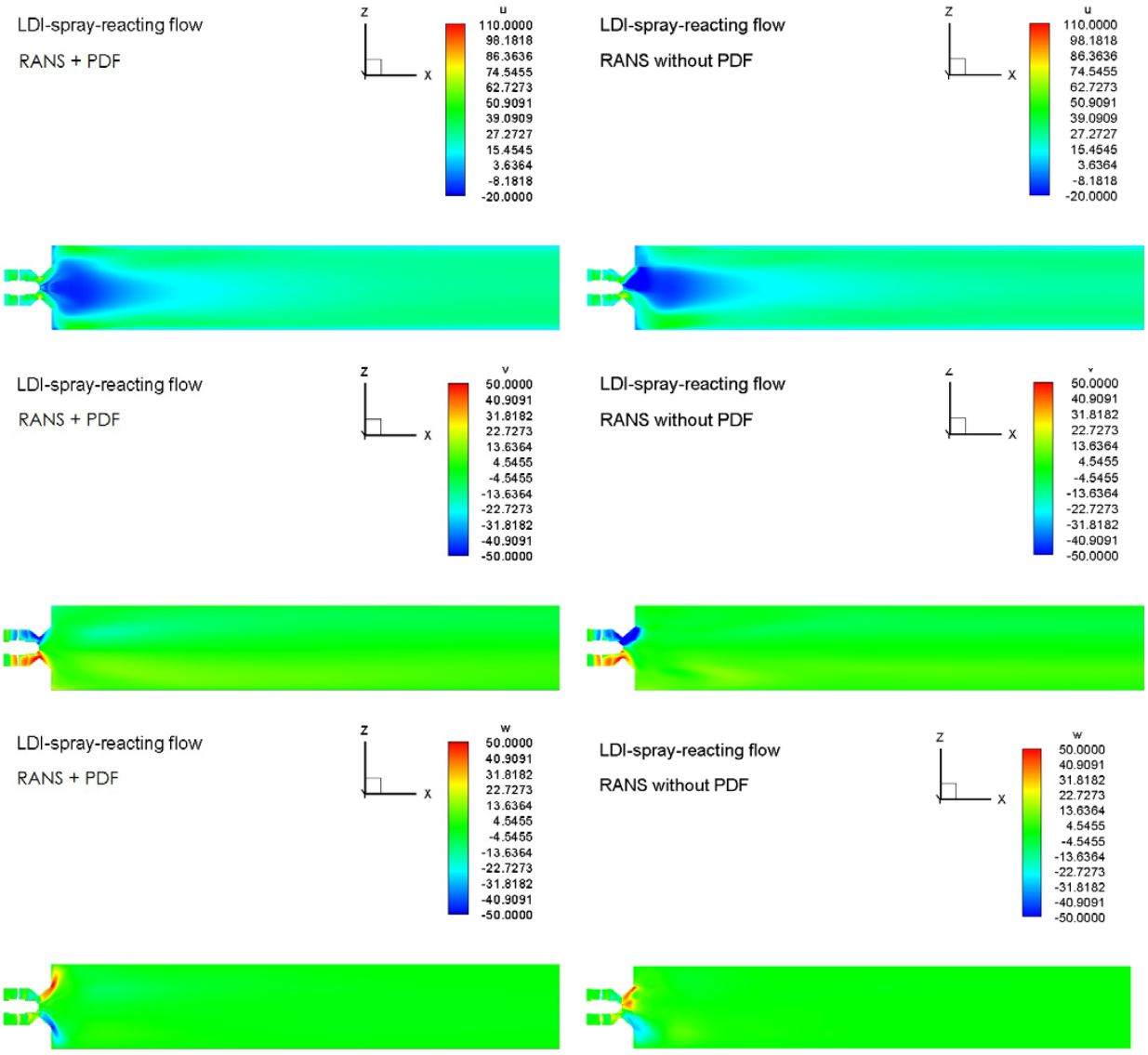

Figure 14.—Comparison of U,V,W contours in center plane.

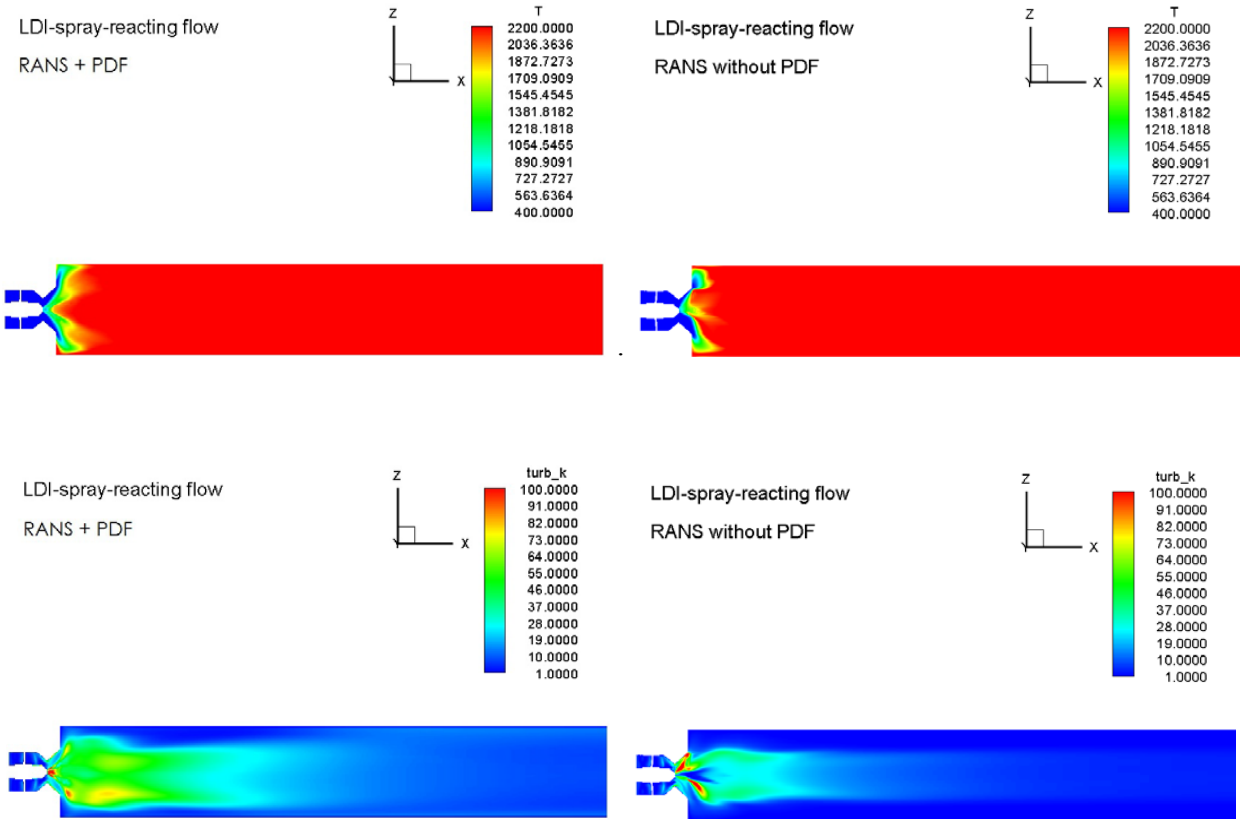

Figure 15.—Comparison of temperature and k contours in center plane.

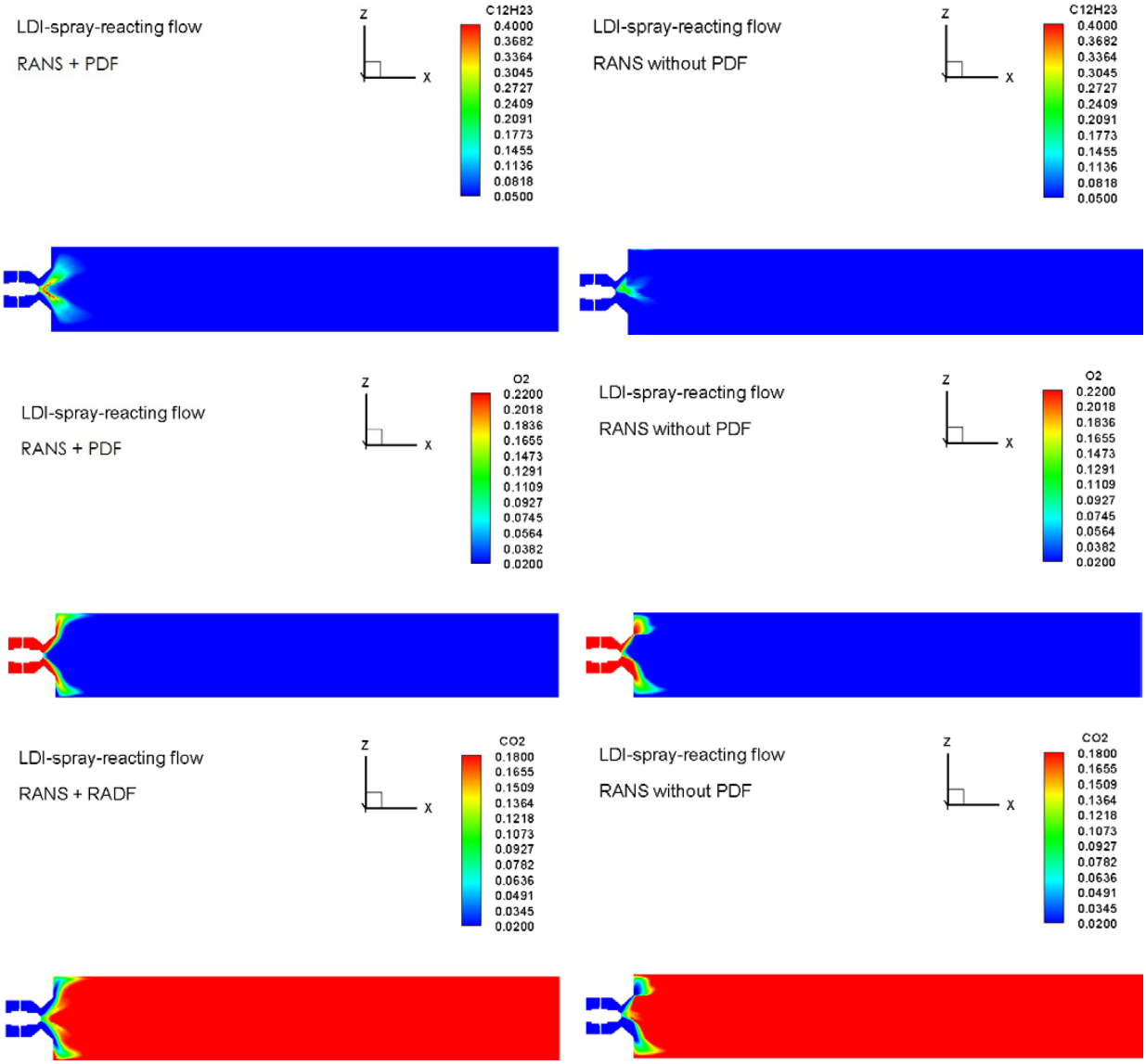

Figure 16.—Comparison of C12H23, O2 and CO2 contours in center plane.

4.2 Results of URANS Simulations With and Without Invoking an Eulerian Scalar APDF

In this section, we present the results of unsteady simulations with and without scalar APDF equation. Most results will be presented in a similar way to what we have done for the steady simulations in Section 4.1. URANS without the scalar APDF equation is carried out up to 83,000 time steps, the size of time step dt = $2.\times10^{-6}$, which is also used in the solvers for spray and scalar APDF equation for synchronizing the simulation. After the simulated flow is fully developed, the mean turbulent quantities are calculated by averaging over the last 20,000 time steps, which is about 2.44 “flow through times” (FTT) which is defined here as the time period that is needed for the flow to go from the inlet to the outlet of the computational domain based on the speed at the inlet. Then the simulation is switched to URANS with the scalar APDF equation and carried out up to 153,000 time steps. Again, the mean values of turbulent quantities are obtained by averaging over the last 20,000 time steps. Figure 17 depicts the global mean structures from abovementioned two unsteady simulations of spray reacting flow.

The main results to be presented are: 1) the convergence history of unsteady simulations, 2) the time histories of velocity components and temperature at four probes along the centerline, 3) the centerline distribution of temperature and axial velocity, 4) the profiles of temperature and velocity components along Z axis at several downstream locations compared with available experimental data, 5) the center recirculation zone and the contour plots of various mean turbulent quantities in the center x-z plane.

4.2.1 Convergence History

Figure 18 shows the time history of the number of subiteration incurred in unsteady simulations with and without invoking the scalar APDF equation over the last 20,000 time steps. It is interesting to see that the simulation with the scalar APDF equation converges much faster than the simulation without the scalar APDF equation. For each time step, the former converges after 21 to 33 subiterations, but the later often needs much more subiterations to converge. Comparing the wall time of computing, the simulation with APDF is about 31 hr with 256 processors for the 20,000 time steps; however, the simulation without APDF needs about 42 hr to finish 20,000 time steps of calculations.

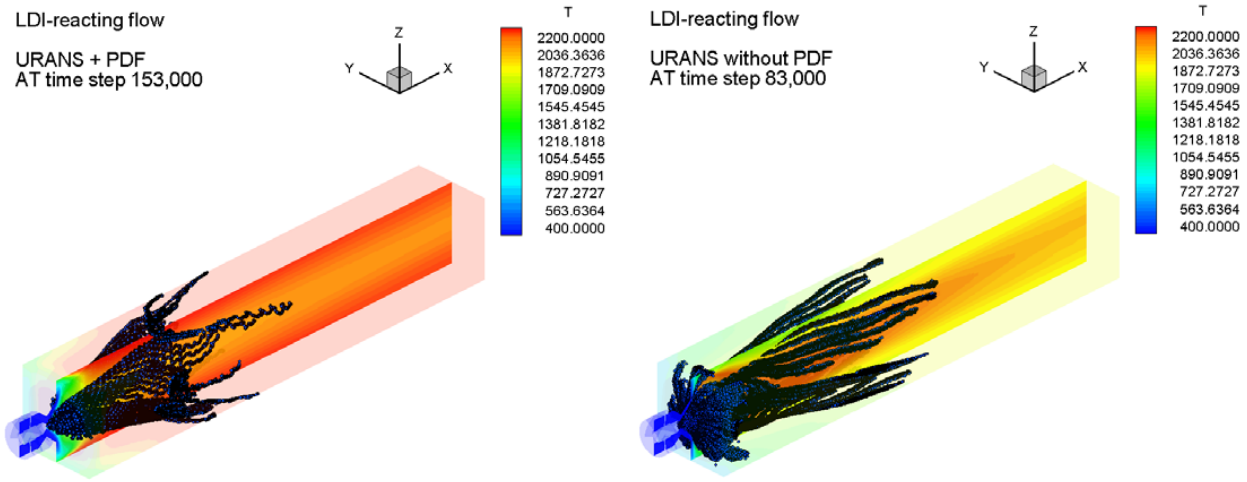

Figure 17.—Global pictures of spray reacting flow simulated with and without scalar PDF method.

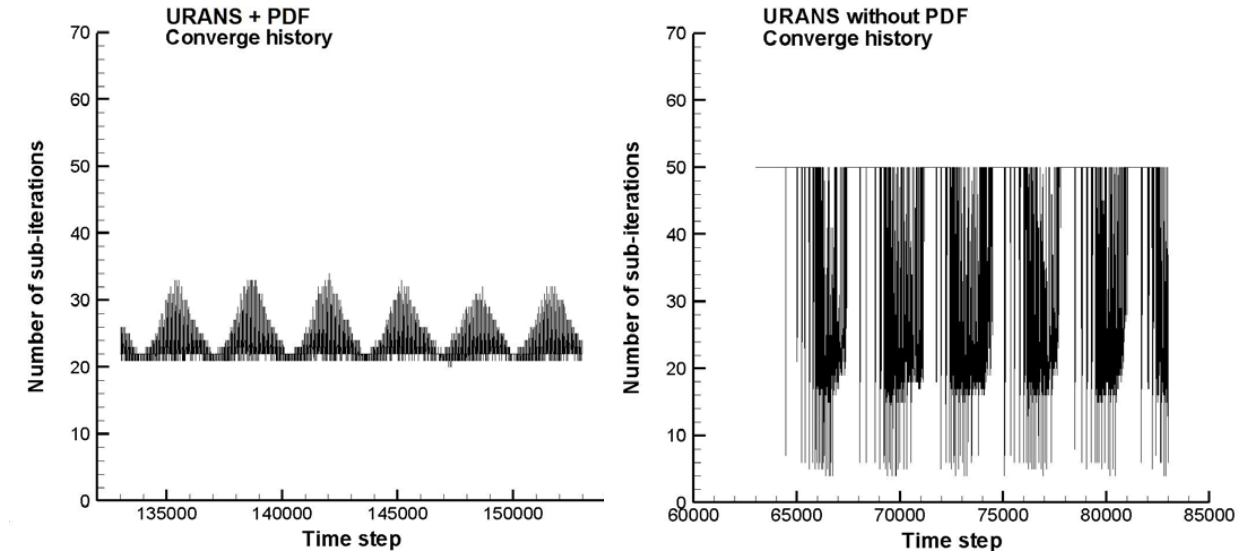

Figure 18.—Convergence histories of unsteady simulations.

4.2.2 Time Variation of Instantaneous Variables at Centerline Probes

Time history of velocity components and temperature at four locations are recorded during the simulation. Here we list the time history at the probes 1, 2, 3, 5 (see Figure 19 and Figure 20), it can be seen that at the first three locations the flow appears to be strongly unsteady and fully developed.

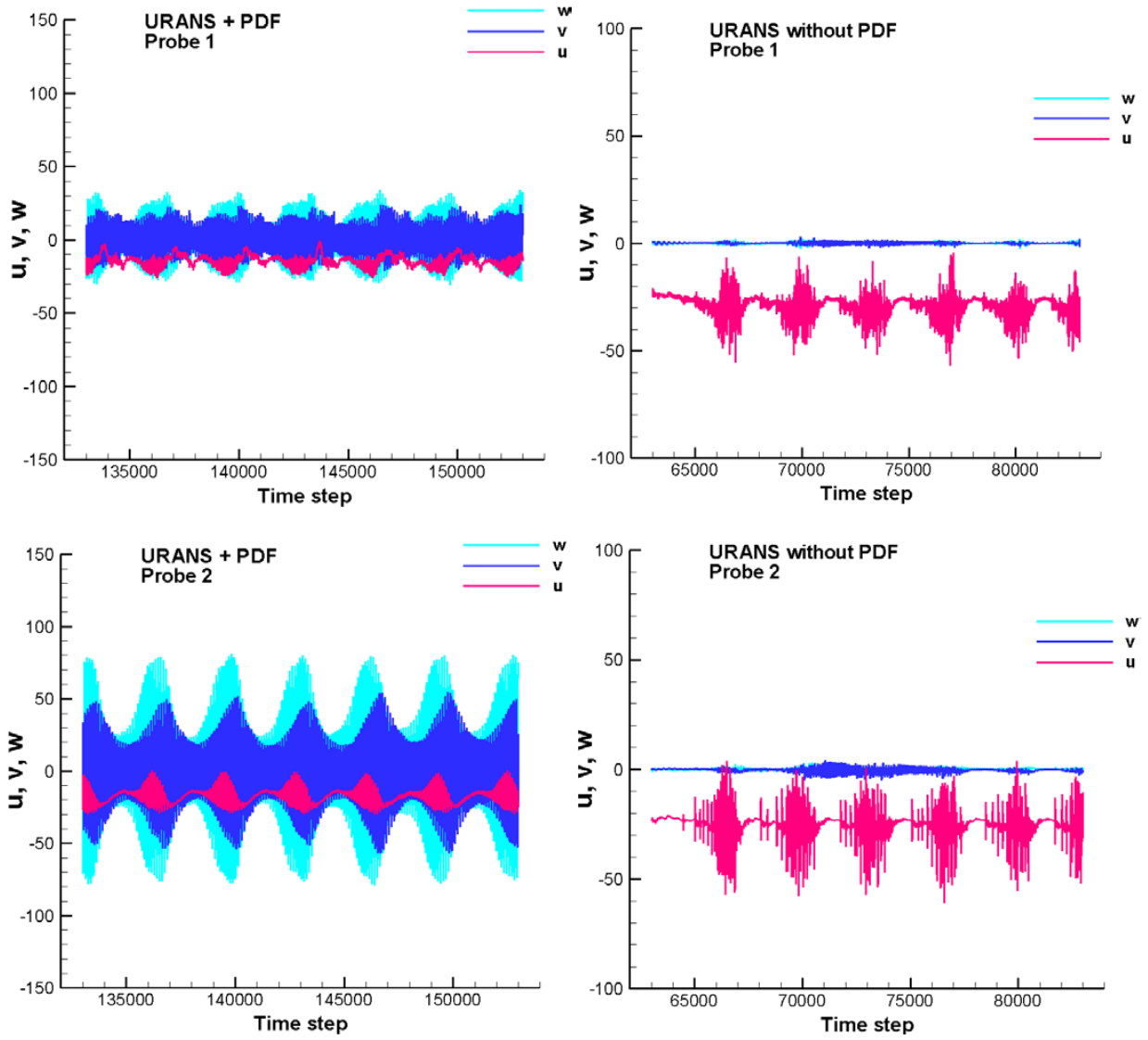

Figure 19.—Time history of velocity components u, v and w at 4 probes.

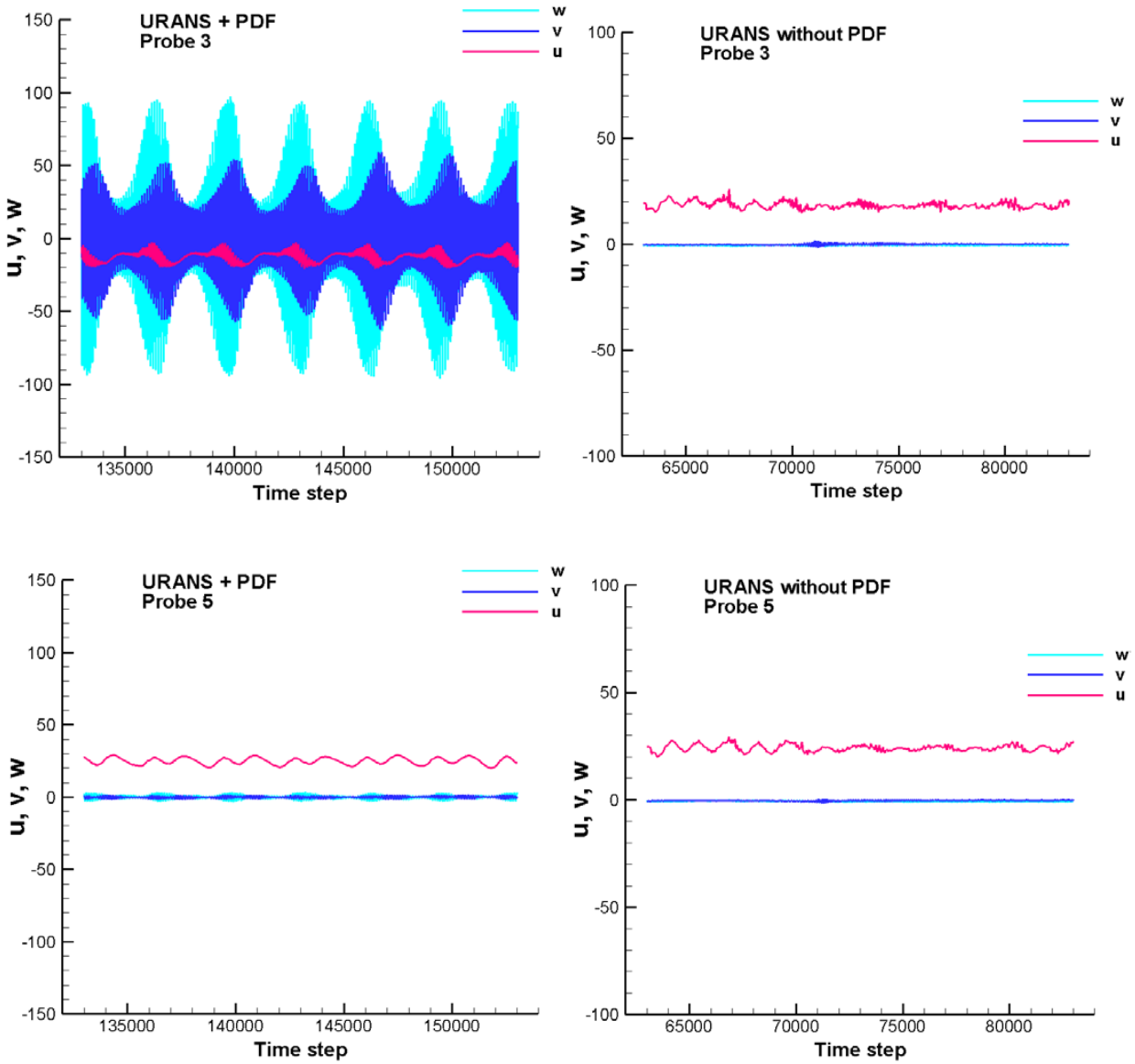

Figure 19.—Concluded.

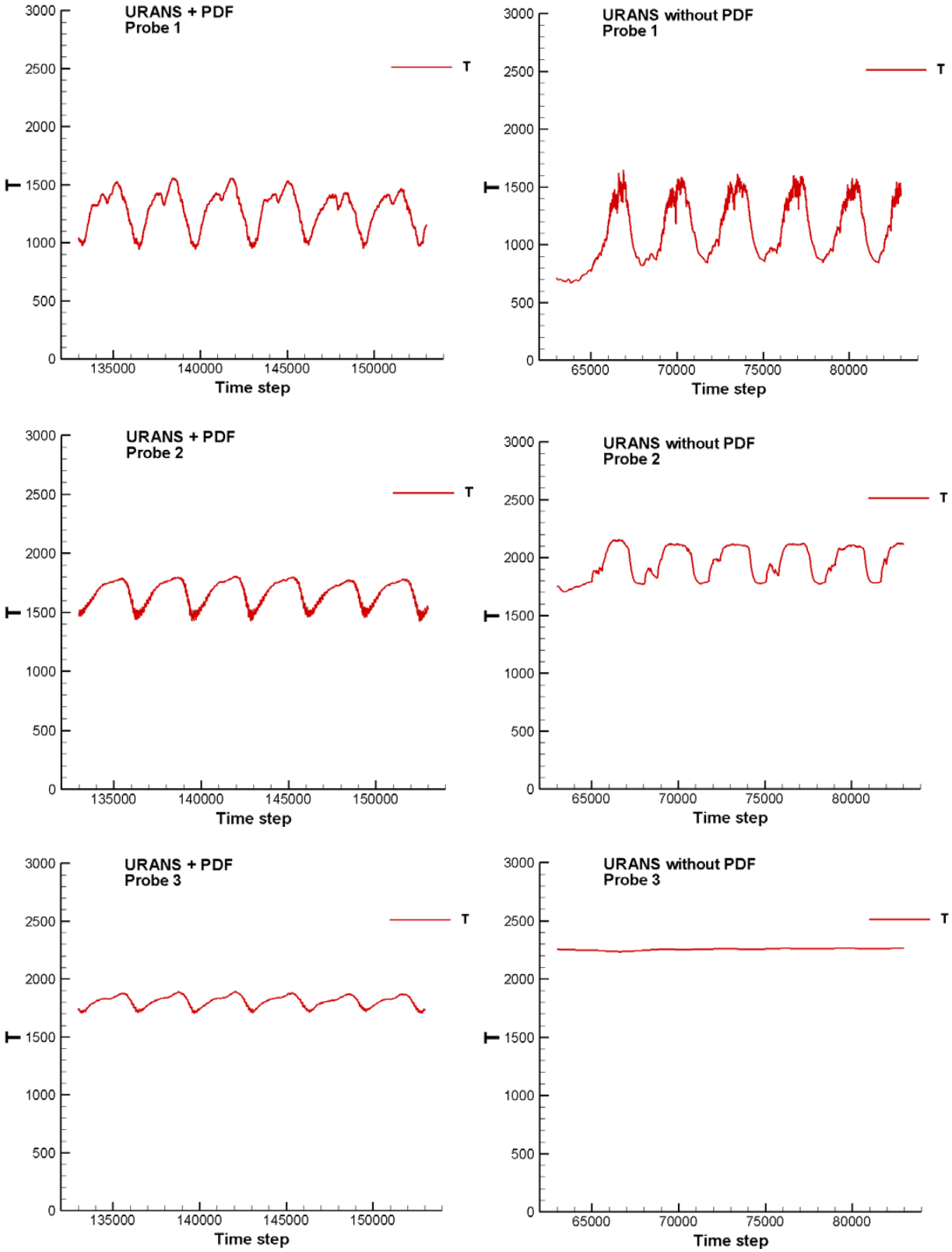

Figure 20.—Time history of temperature at 4 probes.

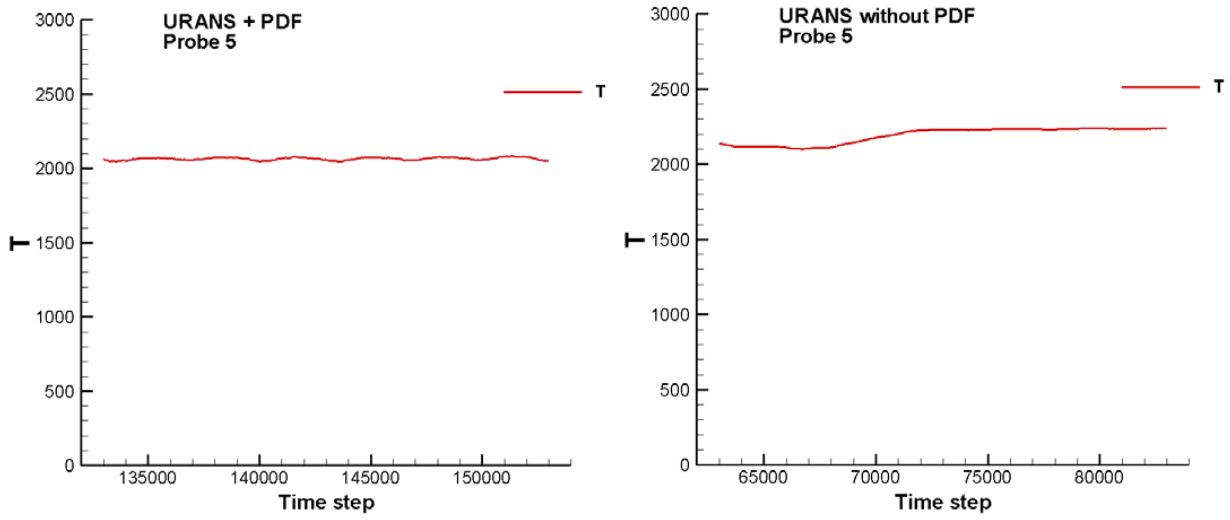

Figure 20.—Concluded.

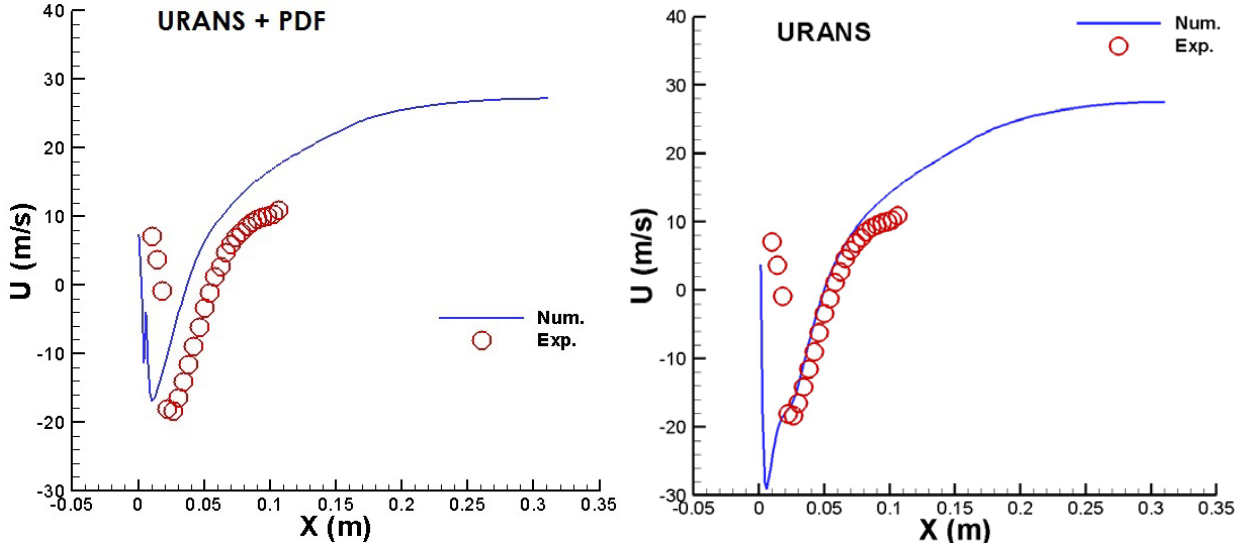

Figure 21.—Centerline distribution of mean axial velocity U.

4.2.3 Centerline Distributions of Mean Temperature and Axial Velocity

Centerline distributions of mean axial velocity and temperature are shown in Figure 20 and Figure 21. The effect of scalar APDF equation on the unsteady simulation is quite similar to the case of steady simulation described in Section 4.1.2.

4.2.4 Mean Temperature and Velocity Profiles Along Z Axis at Downstream Locations

Mean temperature profiles at downstream locations x = 5, 10, 20 and 200mm are compared and shown in Figure 22. These comparisons have revealed a positive effect of the APDF equation on the prediction of temperature. However, the effect of APDF equation on the velocity field, shown in Figure 23 and Figure 24, is not as obvious in present unsteady simulations.

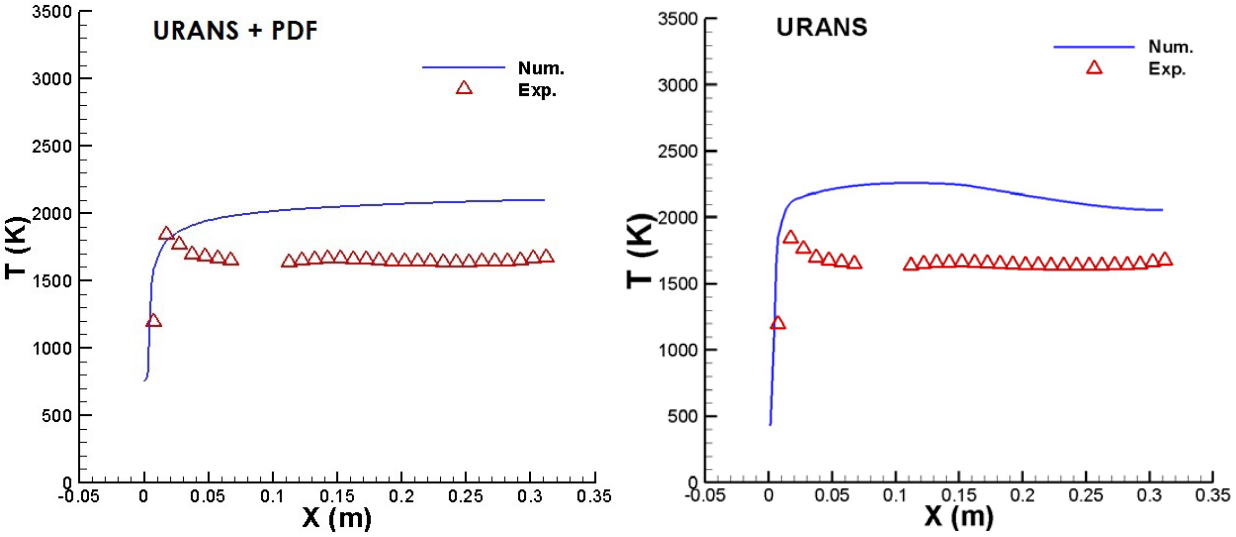

Figure 22.—Centerline distribution of mean temperature T.

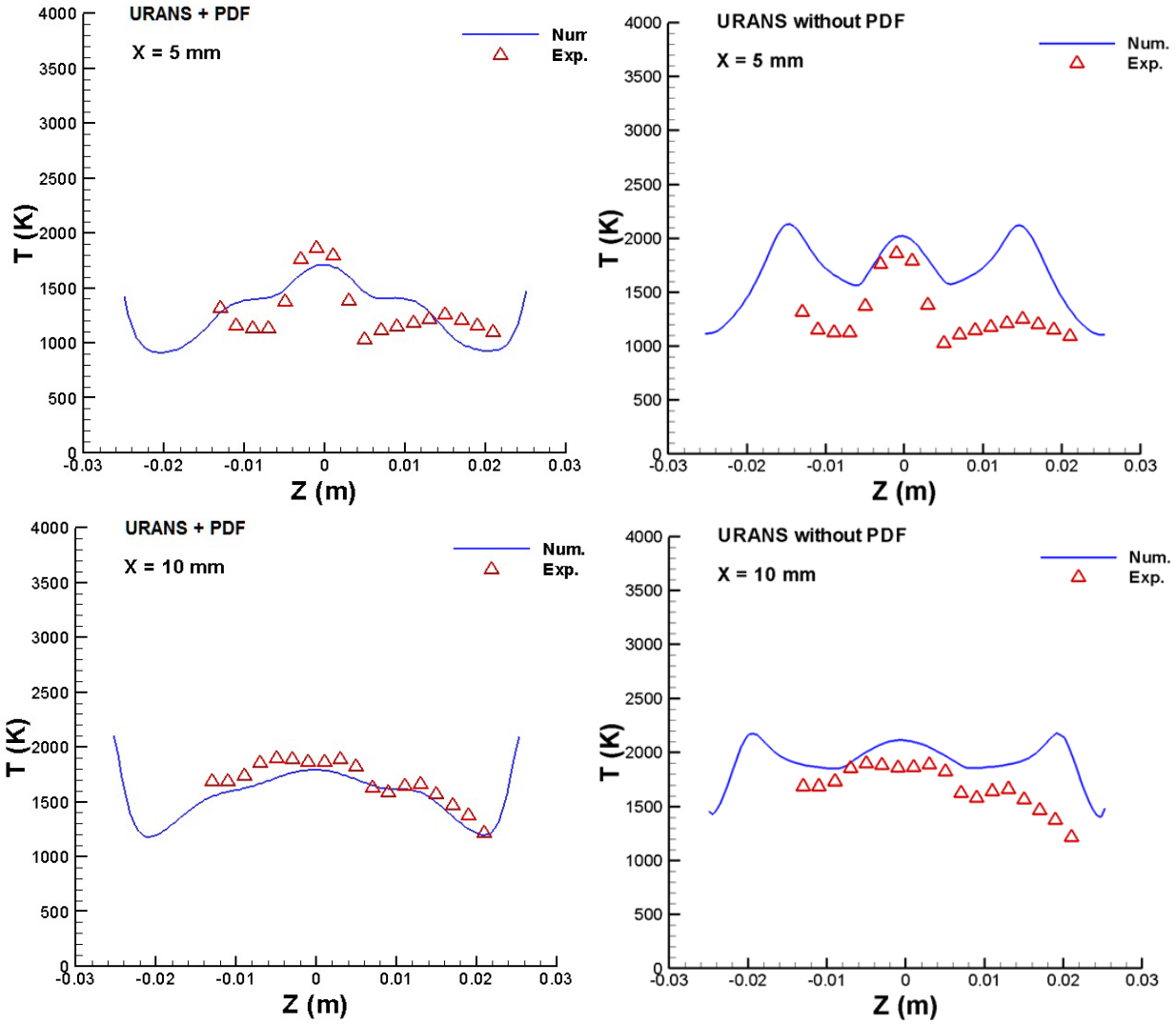

Figure 23.—Comparison of temperature distribution along Z axis at x = 5, 10, 20, 200 mm.

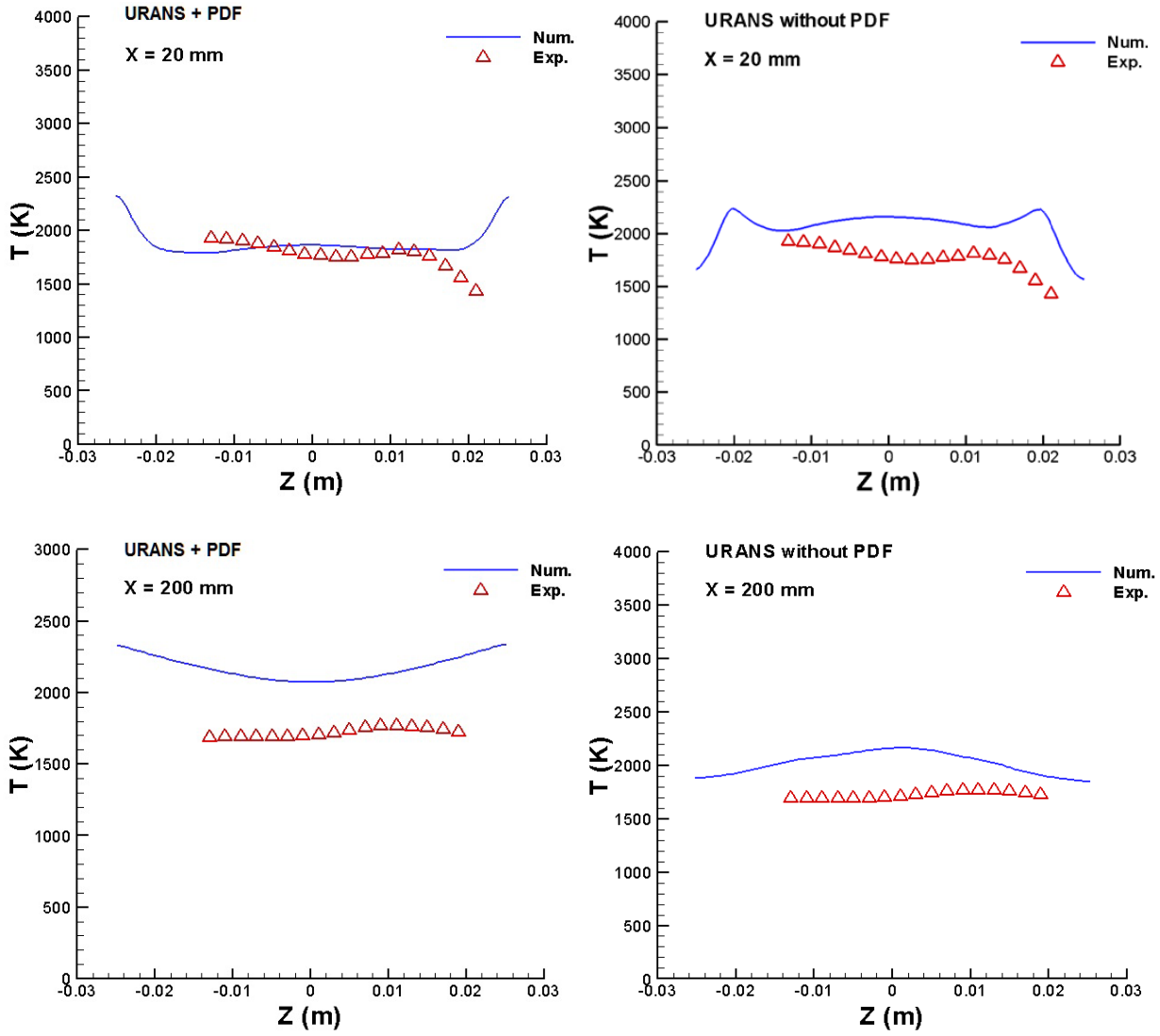

Figure 23.—Concluded.

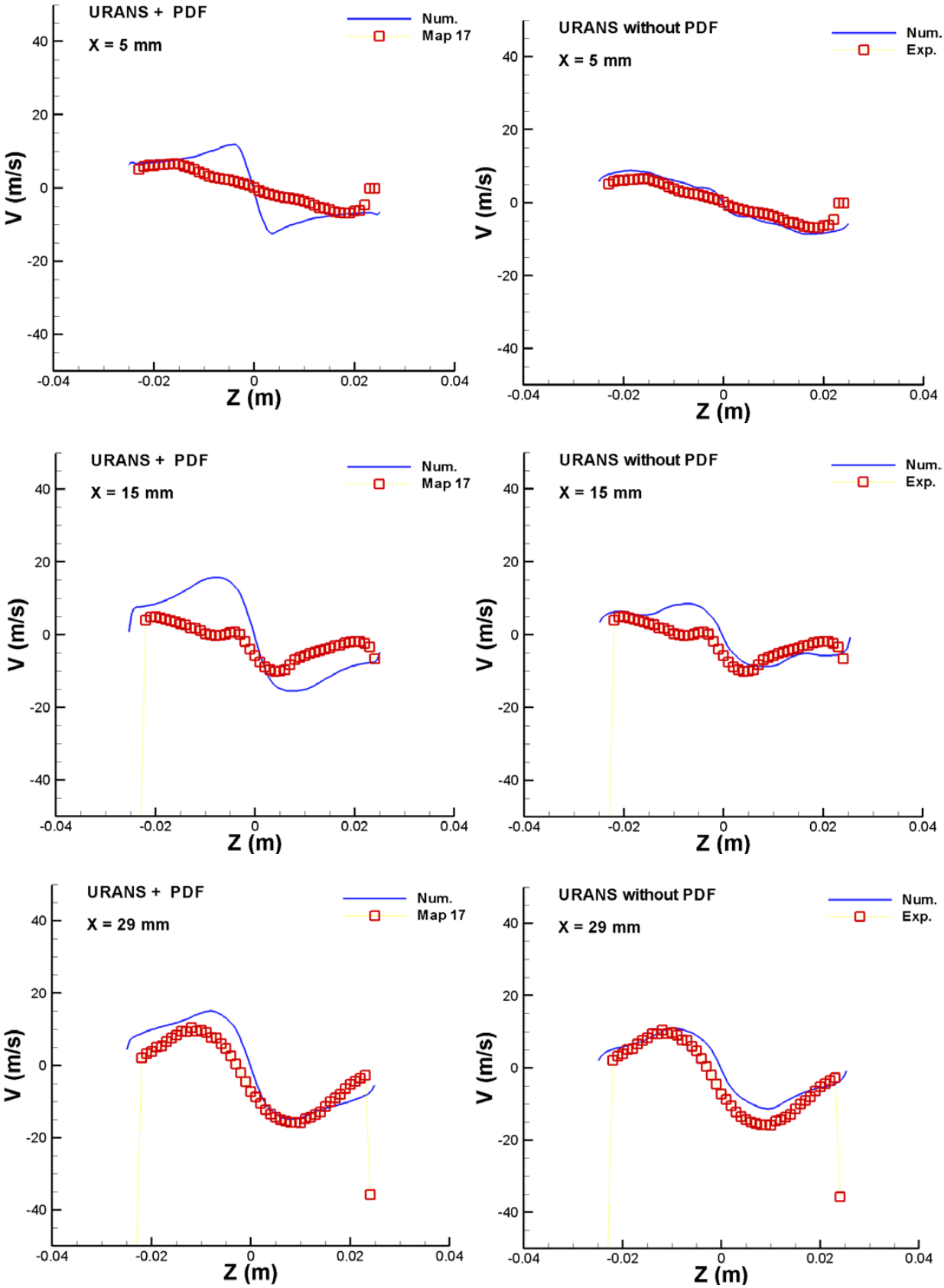

Figure 24.—Comparison of velocity component V along Z axis at x = 5, 15, 29, 38, 92mm.

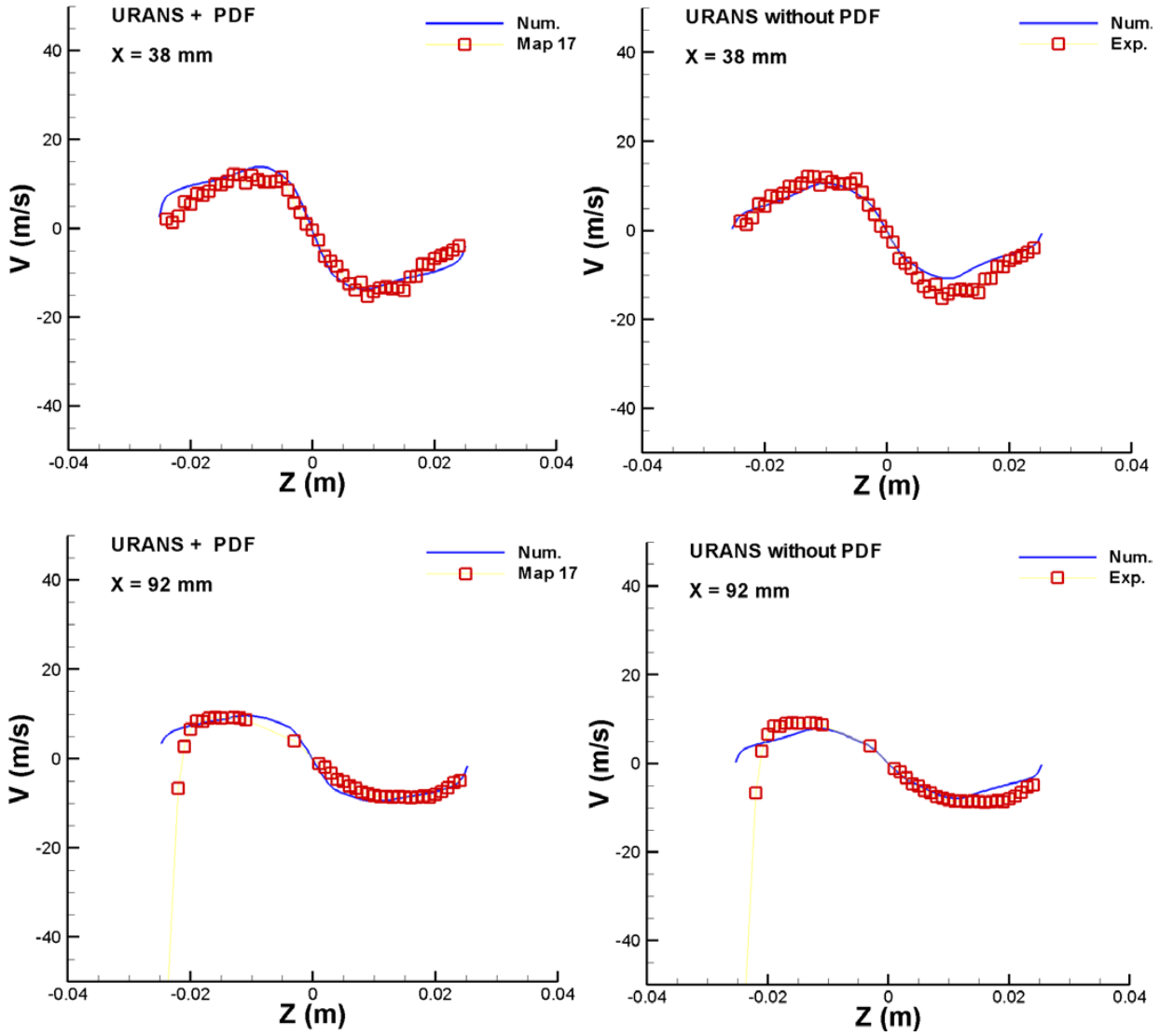

Figure 24.—Concluded.

4.2.5 Flow Structure and Contour Plots of Mean Variables in the Center x-z Plane

To reveal the simulated mean flow and flame structures, we have plotted the center recirculation zone by the isosurface of zero axial velocity (see Figure 25), the contour plots of velocity components, temperature, turbulent kinetic energy and species mass fractions C12H23, O2 and CO2 are shown in Figure 26, Figure 27, and Figure 28. From these figures we observe that the structures of all scalar fields simulated by URANS with the APDF equation are quite different from the ones by URANS without the APDF equation. Also, we notice that the level of turbulent kinetic energy is significantly reduced in the unsteady simulation with the APDF equation (a phenomenon often found in the simulations with the conventional or standard PDF method); however, it does not severely affect the global structure of turbulent reacting flow in our simulations due to, we believe, the use of the APDF equation, in which the time scale or frequency for the APDF diffusion in the sample space is not directly related to the turbulent kinetic energy, instead, it is determined by the strain and rotation rate of the turbulent mean flow (see Eq. (56)).

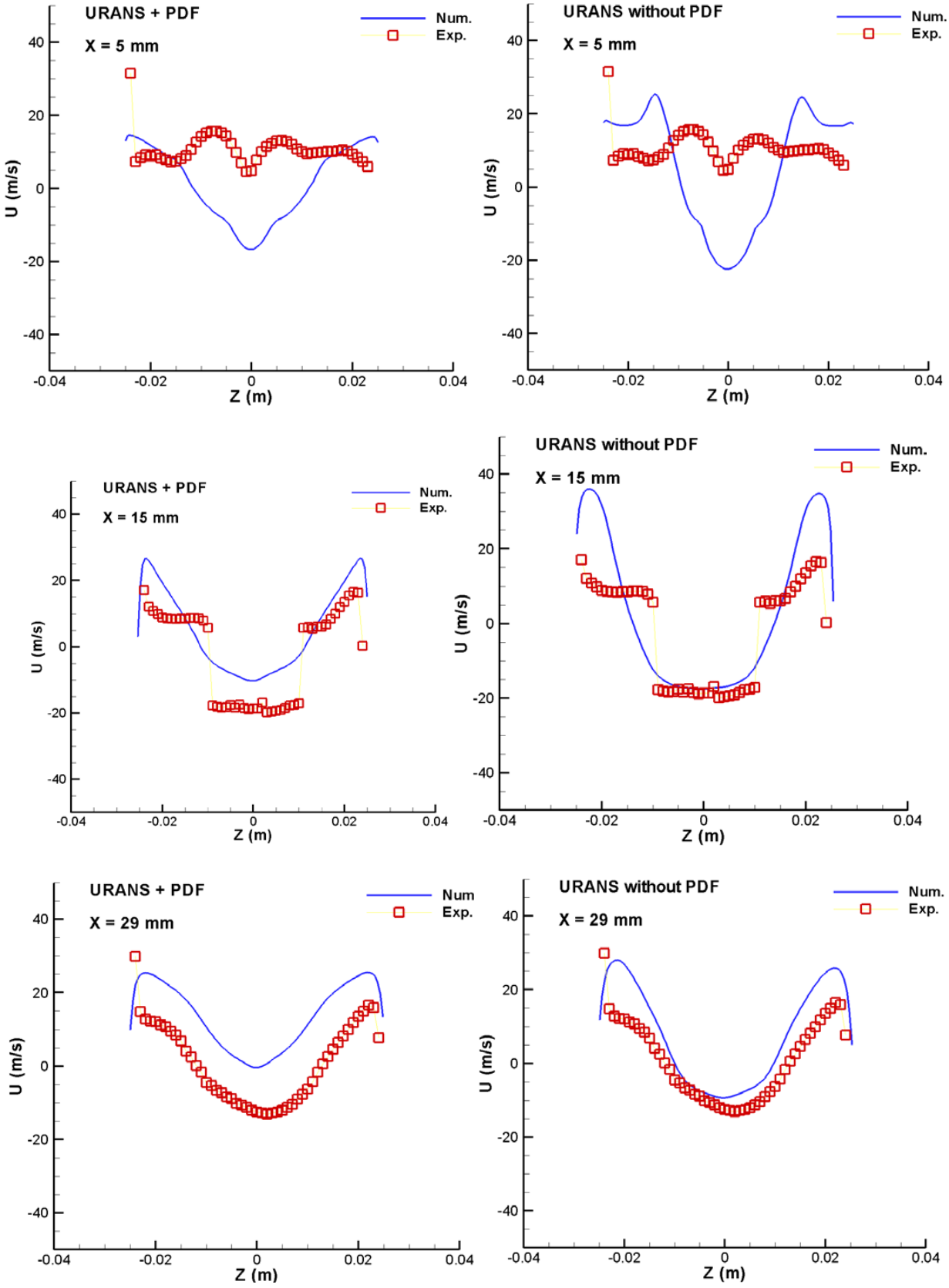

Figure 25.—Comparison of velocity component U along Z axis at x = 5, 15, 29, 38, 92mm.

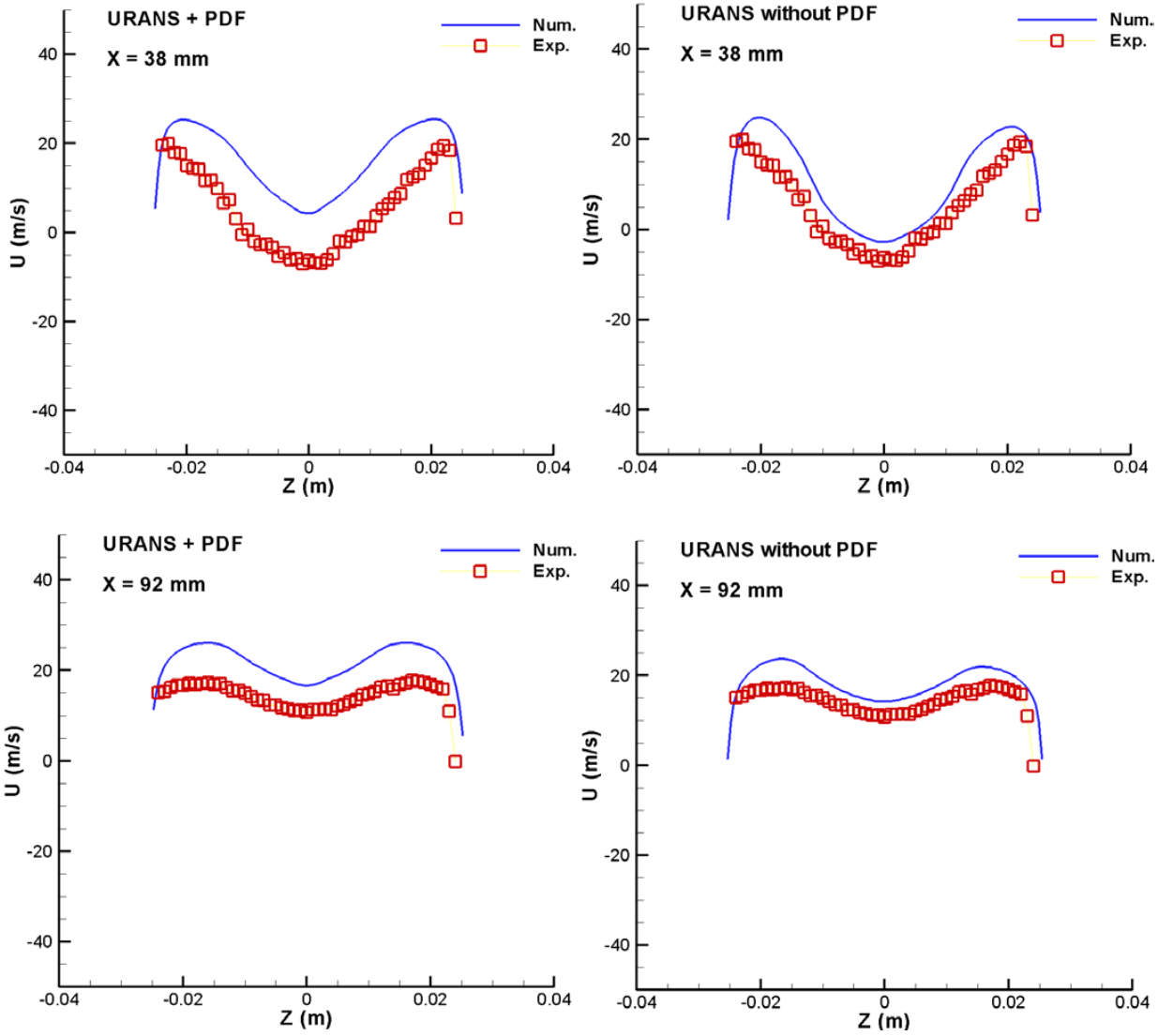

Figure 25.—Concluded.

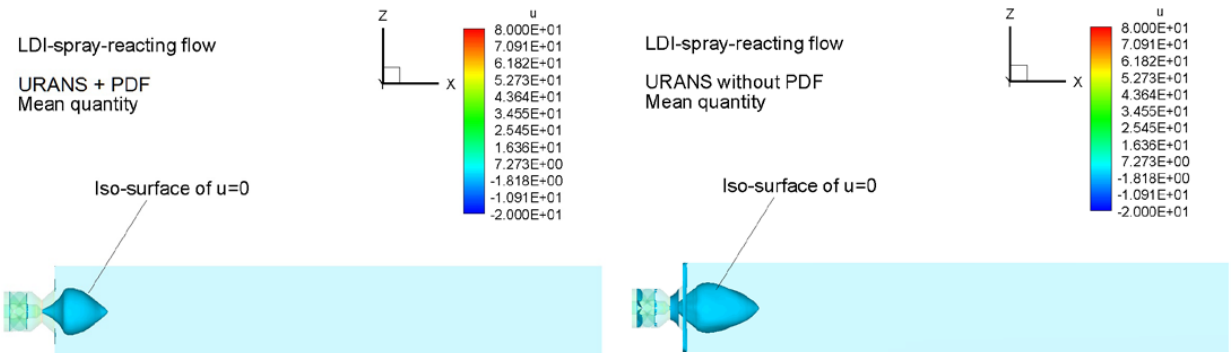

Figure 26.—Comparison of center recirculation zone.

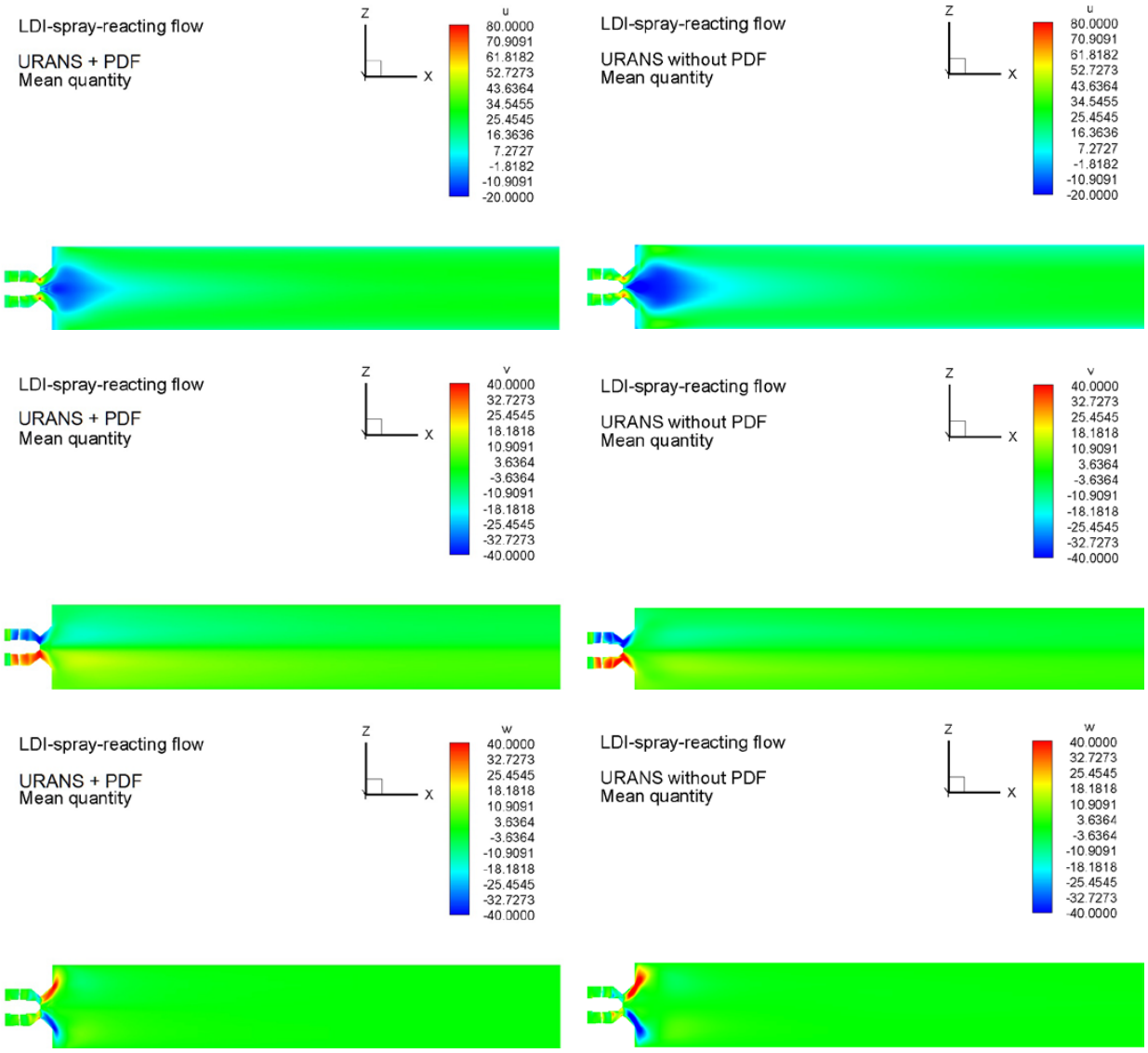

Figure 27.—Comparison of mean velocities U, V, W contours in center plane.

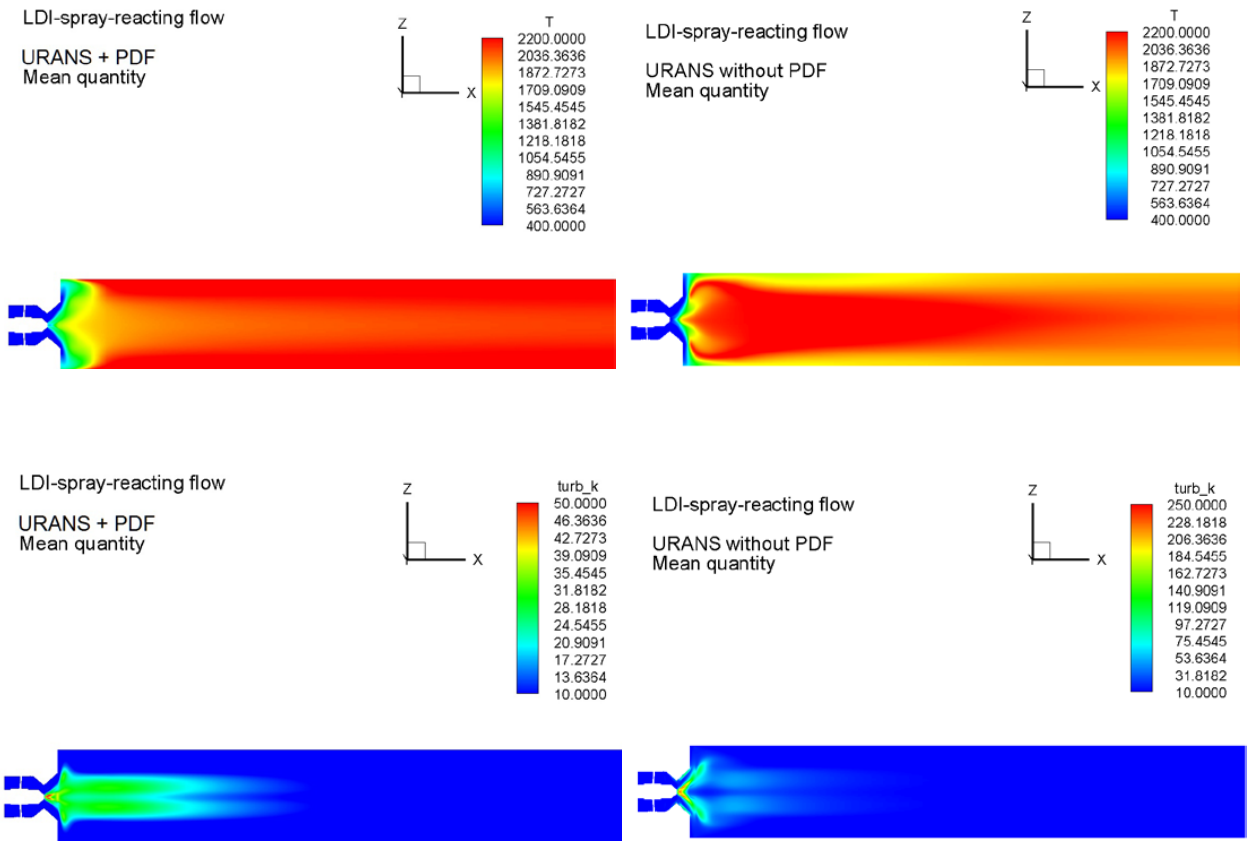

Figure 28.—Comparison of mean temperature and k contours in center plane.

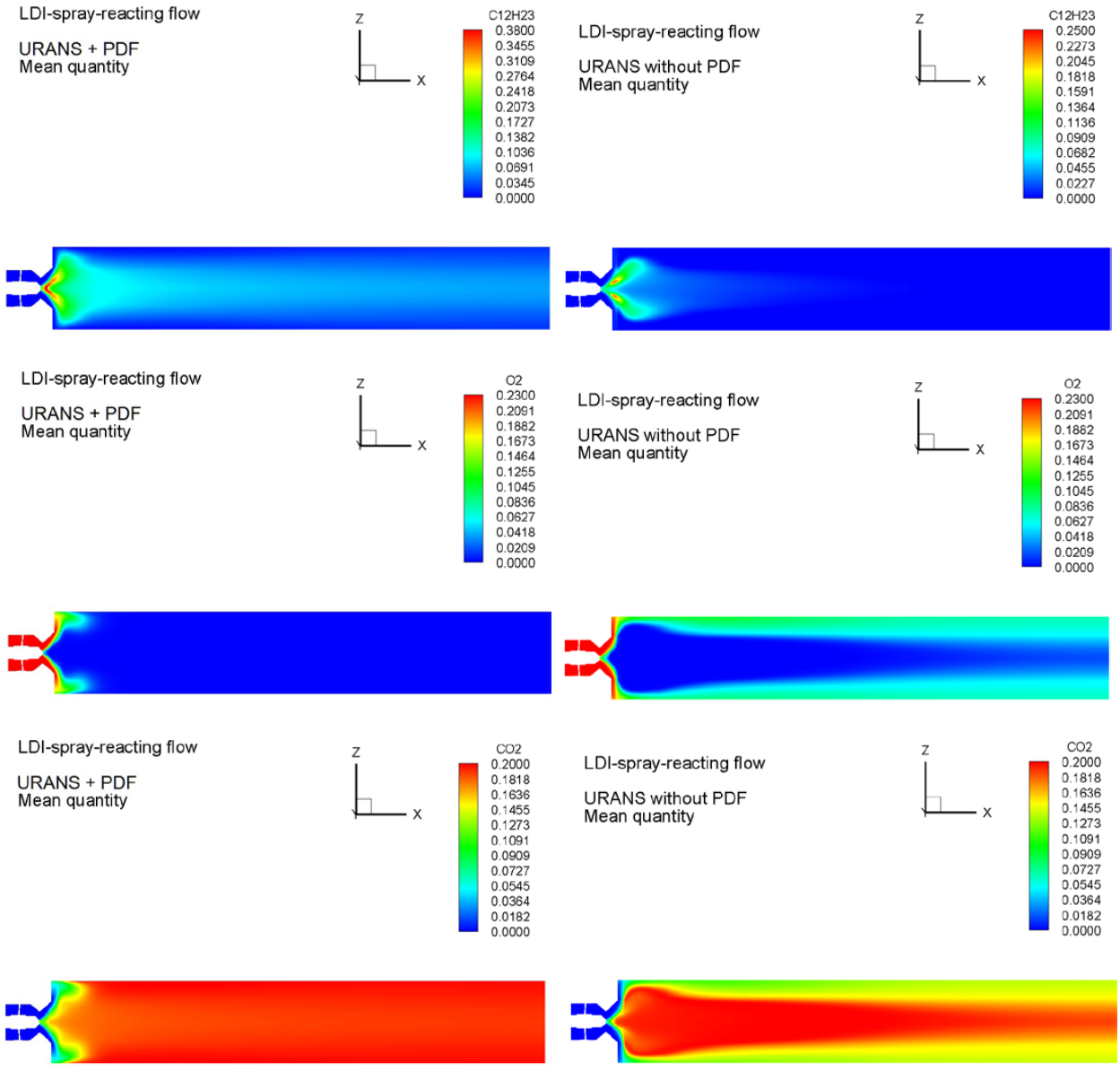

Figure 29.—Comparison of C12H23, O2 and CO2 contours in center plane.

5.0 Conclusions

The numerical simulations of Jet-A spray reacting flow in a single element LDI injector have been carried out both with and without invoking an Eulerian scalar APDF method. The NCC code is used under the same numerical setting, same computational geometry and grid resolution. In addition, the same spray model and the same chemistry kinetics are used for all the steady and unsteady simulations. In this way, we hope to isolate and study only the effect of scalar PDF method (with the scalar APDF equation) on simulations, paying particular attention to the simulation quality and numerical performance (e.g., computational stability and efficiency).

From both steady and unsteady simulations we have observed that there are noticeable improvements achieved on the temperature prediction in the region of strong turbulence by using the scalar PDF method. The distribution or structure of other scalar quantities appears to have significant differences between the

simulations using with and without the scalar APDF equation, and the scalar PDF method seems to produce more reasonable results. However, we need more reliable experimental data for a better evaluation. For the flow field, we also notice a big difference and improvement in the steady simulation with the PDF method, but not much in the unsteady simulation.

As to the numerical performance, the observation is that both steady and unsteady simulations invoking an Eulerian scalar PDF method appear to be more stable and faster than the conventional RANS and URAMS simulations.

Further evaluations of the scalar APDF equation and studies of stochastic numerical procedure for Eulerian scalar PDF method will be continued and extended to the large eddy simulation (LES) approach.

References

1. Pope, S. B, "Turbulent Flows," Cambridge University Press, 2000.
2. Jaberi, F.A., Colucci, P.J., James, S., Givi, P. and Pope, S.B., "Filtered mass density function for Large-eddy simulation of turbulent reacting flows," J. Fluid Mech., vol. 401, pp.85-121, 1999.
3. M.S. Raju, EUPDF-II: "An Eulerian Joint Scalar Monte Carlo PDF Module Users' Manual," NASA/CR—2004-213073.
4. Liu, N.-S., "On the Comprehensive Modeling and Simulation of Combustion Systems," AIAA-2001-0805, January 2001.
5. Liu, N.-S., and Shih, T.-H., "Turbulence Modeling for Very Large-Eddy Simulation," *AIAA Journal,* Vol. 44, No. 4, 2006, pp. 687-697.
6. Shih, T.-H., and Liu, N.-S., "A non-linear Dynamic Subscale Model for Partially Resolved Numerical Simulation (PRNS)/Very Large Eddy Simulation (VLES) of Internal Non-Reacting Flows," NASA/TM—2010-216323, May 2010.
7. Shih, T.-H. and Liu, N.-S., "Ensemble Averaged Probability Density Function (APDF) Equations for Compressible Turbulent Reacting flows," NASA/TM (submitted).
8. Iannetti, A.C. and Liu, N.-S., "Effect of Spray Initial Conditions on Heat Release and Emissions in LDI CFD Calculations," AIAA-2008-1150, January 2008.
9. Tennekes, H. and Lumley, J. L., A FIRST COURSE IN TURBULENCE, The MIT Press, 1972.
10. Baldwin, B.S. and Lomax, H., "Thin Layer Approximation and Algebraic Model for Separated Turbulent Flows," 1978. AIAA paper 78-257.
11. Speziale, C. G., "Turbulence Modeling for Time-Dependent RANS and VLES: A Review," AIAA J., Vol. 36, No.2, 1998.
12. Shih, T.-H., Zhu, J., Liou, W., Chen, K.-H., Liu, N.-S. and Lumley, J. L., " Modeling of Turbulent Swirling Flows," NASA/TM—1997-113112, 1997.
13. Shih, T.-H., "Constitutive Relations and Realizability of Single-Point Turbulence Closures" Turbulence and Transition Modelling, Chapter 4., Edited by Hallback, M., Henningson, D.S., Johansson, A.V. and Alfredsson, P.H., KLUWER ACADEMIC PUBLISHERS, 1996.
14. Shih, T.-H., "Some developments in computational modeling of turbulent flows," Fluid Dynamic Research 20 (1997) 67-96.
15. Shih, T.-H., Liou, W.W., Shabbir, A., Yang, Z. and Zhu, J., "A New $k-\varepsilon$ Eddy Viscosity Model for High Reynolds Number Flows," Computational Fluids, Vol.24, No.3, pp227-238, 1995.
16. Shih, T-H. and Liu, N.-S., "Conservational PDF Equations of Turbulence," NASA/TM—2010-21638.
17. Davoudzadeh, F., Liu, N.-S. and Moder, J. P., "Investigation of Swiring Air Flows Generated by axial Swirlirs in a Flame Tube," Proceedings of GT2006 ASME Turbo Expo 2006: Power for Land, Sea, and Air May 8-11, 2006, Barcelona, Spain.
18. Cai, J., Jeng, S.-M., and Tacina, R., "The Structure of A Swirl-Stablized Reacting Spray Issued from An Axial Swirler," AIAA-2005-1424, 43rd AIAA Aerospace Science Meeting and Exhibit, 10-13 January 2005, Reno, NV.

REPORT DOCUMENTATION PAGE	Form Approved OMB No. 0704-0188

1. REPORT DATE *(DD-MM-YYYY)*	2. REPORT TYPE	3. DATES COVERED *(From - To)*
01-08-2012	Technical Memorandum	

4. TITLE AND SUBTITLE
Simulations of Spray Reacting Flows in a Single Element LDI Injector With and Without Invoking an Eulerian Scalar PDF Method

5a. CONTRACT NUMBER

5b. GRANT NUMBER

5c. PROGRAM ELEMENT NUMBER

6. AUTHOR(S)
Shih, Tsan-Hsing; Liu, Nan-Suey

5d. PROJECT NUMBER

5e. TASK NUMBER

5f. WORK UNIT NUMBER
WBS 561581.02.08.03.44.02;
984754.02.07.03.19.02

7. PERFORMING ORGANIZATION NAME(S) AND ADDRESS(ES)
National Aeronautics and Space Administration
John H. Glenn Research Center at Lewis Field
Cleveland, Ohio 44135-3191

8. PERFORMING ORGANIZATION REPORT NUMBER
E-18351

9. SPONSORING/MONITORING AGENCY NAME(S) AND ADDRESS(ES)
National Aeronautics and Space Administration
Washington, DC 20546-0001

10. SPONSORING/MONITOR'S ACRONYM(S)
NASA

11. SPONSORING/MONITORING REPORT NUMBER
NASA/TM-2012-217676

12. DISTRIBUTION/AVAILABILITY STATEMENT
Unclassified-Unlimited
Subject Categories: 01 and 64
Available electronically at http://www.sti.nasa.gov
This publication is available from the NASA Center for AeroSpace Information, 443-757-5802

13. SUPPLEMENTARY NOTES

14. ABSTRACT
This paper presents the numerical simulations of the Jet-A spray reacting flow in a single element lean direct injection (LDI) injector by using the National Combustion Code (NCC) with and without invoking the Eulerian scalar probability density function (PDF) method. The flow field is calculated by using the Reynolds averaged Navier-Stokes equations (RANS and URANS) with nonlinear turbulence models, and when the scalar PDF method is invoked, the energy and compositions or species mass fractions are calculated by solving the equation of an ensemble averaged density-weighted fine-grained probability density function that is referred to here as the averaged probability density function (APDF). A nonlinear model for closing the convection term of the scalar APDF equation is used in the presented simulations and will be briefly described. Detailed comparisons between the results and available experimental data are carried out. Some positive findings of invoking the Eulerian scalar PDF method in both improving the simulation quality and reducing the computing cost are observed.

15. SUBJECT TERMS
Combustion CFD

16. SECURITY CLASSIFICATION OF:			17. LIMITATION OF ABSTRACT	18. NUMBER OF PAGES	19a. NAME OF RESPONSIBLE PERSON
a. REPORT	b. ABSTRACT	c. THIS PAGE			STI Help Desk (email:help@sti.nasa.gov)
U	U	U	UU	50	19b. TELEPHONE NUMBER *(include area code)* 443-757-5802